

FULL ARTICLE

## Channel-specific core-valence projectors for determining partial Auger decay widths

Florian Matz<sup>a</sup> and Thomas-Christian Jagau<sup>a</sup>

<sup>a</sup>Division of Quantum Chemistry and Physical Chemistry, KU Leuven, Celestijnenlaan 200F, 3001 Leuven, Belgium.

### ARTICLE HISTORY

Compiled May 24, 2022

### ABSTRACT

Auger decay is a relaxation process of core-vacant states in atoms and molecules, in which one valence electron fills the core vacancy while a second one is emitted. These states pose a challenge to electronic-structure theory, because they are embedded in the ionization continuum. Recently, we showed that molecular Auger decay can be described using complex-variable coupled-cluster (CC) methods and that partial widths and branching ratios can be computed based on a decomposition of the CC energy. Here, we introduce channel-specific core-valence projectors, dubbed Auger channel projectors, as a more general technique to evaluate partial widths from complex-variable treatments. We apply this new method to core-ionized states of neon, water, ammonia, and methane using CC singles and doubles (CCSD), equation-of-motion ionization potential CCSD, and configuration interaction singles (CIS) wave functions. Even though a single CIS calculation can never describe all Auger decay channels at once, we show that a combination of CIS calculations based on different reference states is able to recover partial and total decay widths from CC calculations to an excellent degree.

### KEYWORDS

Auger decay; electronic resonances; coupled-cluster; configuration interaction singles; electronic structure

## 1. Introduction

Auger decay is the most important relaxation process for core vacancies in systems with light nuclei [1]. It is common in systems irradiated by X-rays or high-energy electrons where it causes secondary electron emission. These mechanisms can lead to complicated electronic and photonic spectra with many features that are of high interest for analytic methods [1]. However, spectra alone can only give limited information about the mechanisms at play when not supported by a theoretical description that allows the assignment of signals to different electronic transitions. Consequently, core-ionized states and Auger decay have attracted considerable interest in molecular electronic-structure theory.

A fundamental challenge is that core-ionized states are electronic resonances embedded in the ionization continuum [2]; their lifetime is finite precisely because of Auger decay. To model only the energy levels of the species involved in X-ray absorption or Auger spectra, that is, to reproduce the positions of the signals, it has been shown that the decay process can often be neglected. This can be done by means of the core-valence

separation [3] (CVS), which removes from the wave function those configurations that describe the decay. Electronic-structure methods used with CVS projectors include in particular algebraic diagrammatic construction (ADC) [4, 5], coupled-cluster (CC) [6], and equation-of-motion coupled-cluster (EOM-CC) methods [7–9].

To actually describe Auger decay, one needs a more elaborate approach to treat the interaction of the metastable core-vacant state with the continuum. Corresponding approaches can be based on the R-matrix method [10–12] or the theory of electronic resonances by Fano [13] and Feshbach [14]. Here, the Hilbert space is partitioned into a bound and a continuum part and the outgoing Auger electron is represented either implicitly using Stieltjes imaging [15–19] or explicitly where its wave function is approximated as a plane wave, Coulomb wave or scattered molecular wave [20–26]. These approaches have the advantage that electronic-structure methods for bound states can be used to describe the initial and final states of Auger decay, but modeling the wave function of the outgoing electron correctly can be challenging [22, 26].

Complex-variable techniques based on non-Hermitian quantum chemistry [2, 27, 28] offer an alternative framework for the treatment of Auger decay [29]. Here, electronic resonances are described as discrete  $L^2$  integrable solutions of the Schrödinger equation with complex energy  $E_{\text{res}} = E - i\Gamma/2$ , where  $E$  is the physical energy of the state and  $\Gamma$  its decay width. In our earlier work [29], we used complex scaling of the Hamiltonian [30, 31] and of the exponents of the basis functions [32, 33] to describe molecular Auger decay. This allows a more black-box approach in the sense that no explicit treatment of the continuum is necessary but the computational cost is increased because of unphysical parameter dependencies [2, 28].

A special interest in the context of Auger decay lies in determining the probability with which a core-ionized state decays into a certain final state. This is usually quantified in terms of partial widths  $\Gamma_i$ , which add up to the total width  $\Gamma$  [1]. Partial widths determine the signal intensities in Auger spectra but they are also relevant because only certain final states of Auger decay can undergo further decay processes such as intermolecular Coulombic decay (ICD) [34] or electron-transfer mediated decay (ETMD) [35].

In our previous work [29], we showed that one can decompose the imaginary part of the energy from a complex-variable CC singles and doubles (CCSD) calculation into contributions from different excitations that can be associated with the decay channels. This allowed the evaluation of partial decay widths from such calculations. However, a similar decomposition of the equation-of-motion ionization potential (EOMIP)-CCSD energy gave bad results.

In the present work, we introduce Auger channel projectors (ACPs) as a more general technique to extract partial decay widths from complex-variable calculations. ACPs are similar to CVS projectors but applied only to individual decay channels. They enable accurate calculations of partial decay widths from CCSD, EOM-CCSD, and configuration interaction singles (CIS) wave functions and may potentially be applied to other wave functions as well. A more detailed discussion of the theory of ACPs is given in Sec. 2, whereas Sec. 3 presents numerical results for core-ionized water and Sec. 4 further applications to neon, ammonia, and methane. Some general conclusions are provided in Sec. 5.

## 2. Theory

### 2.1. Describing Auger decay with complex-variable methods

General overviews of complex scaling can be found, for example, in Refs. [2, 27]. Our approach to molecular Auger decay is based on the method of complex basis functions [32, 33, 36], which is a variant of complex scaling suitable for molecular electronic resonances. In this method, the exponents of several basis functions are multiplied by a complex number  $e^{-2i\theta}$  with  $\theta$  as scaling angle. While it can be shown that the complex resonance energies  $E_{\text{res}} = E - i\Gamma/2$  are independent of  $\theta$  in the basis-set limit,  $E_{\text{res}}$  does depend on  $\theta$  in actual calculations with a finite basis set. In accordance with previous work, we determine the optimal value of  $\theta$  by minimizing  $|dE/d\theta|$  [37, 38]. For this purpose, trajectories  $E(\theta)$  need to be calculated.

We discussed the application of complex-scaled methods to Auger decay in detail in our preceding work [29]. It is necessary to include in the wave function for a core-ionized state configurations in which the core vacancy is filled by one valence electron and another valence electron is emitted into the continuum. The latter is represented in complex-scaled methods by the excitation of an electron into a virtual orbital with a high real energy and a significant imaginary energy [29].

We showed [29] that  $\Delta\text{CCSD}$  [39–41] and EOMIP-CCSD [41–43] yield accurate total and partial Auger decay widths and discussed the strengths and weaknesses of these methods. In the  $\Delta\text{CCSD}$  approach, the neutral ground state of the system and the core-ionized decaying state are described independently from each other by two CCSD wave functions. All final states of Auger decay are double excitations with respect to the core-ionized reference determinant  $|\Psi_0\rangle$  and thus included in the CCSD wave function. This is illustrated for an exemplary four-orbital system in the upper panel of Figure 1. While all determinants included in this wave function have  $M_S = 1/2$ , a further distinction is possible when not taking into account the outgoing electron in the virtual orbital: There are closed-shell determinants (marked in purple), high-spin determinants (marked in red) that represent a triplet final state, and low-spin open-shell determinants (marked in blue) that can be linearly combined to form either a singlet or a triplet final state. Only when neglecting the outgoing electron is the description of the final states spin-complete.

An alternative approach is EOMIP-CCSD, where the wave function of the core-ionized state is constructed by applying a linear excitation operator to a CCSD wave function for the neutral ground state. In EOMIP-CCSD, this operator consists of 1-hole and 2-hole-1-particle excitations. As illustrated in the lower panel of Figure 1, all Auger decay channels can be written as 2-hole-1-particle excitations starting from the neutral ground state and are thus included in the EOMIP-CCSD wave function. The same classification of the decay channels as in CCSD is possible and represented in Figure 1 by the same colors. However, in contrast to an open-shell CCSD approach, the EOMIP-CCSD wave function is by construction a spin eigenfunction.

In our previous work [29], we demonstrated that a main advantage of  $\Delta\text{CCSD}$  over EOMIP-CCSD is that partial decay widths can be evaluated from contributions  $\text{Im}[t_{ij}^{ab} \langle ij || ab \rangle]$  to the imaginary part of the energy where  $i$  and  $j$  are valence orbitals,  $a$  is the core hole, and  $b$  is any virtual orbital representing the state of the outgoing Auger electron. For an EOMIP-CCSD wave function, a similar energy decomposition leads to artificially large partial widths even though total decay widths are not less accurate than those calculated with CCSD [29].

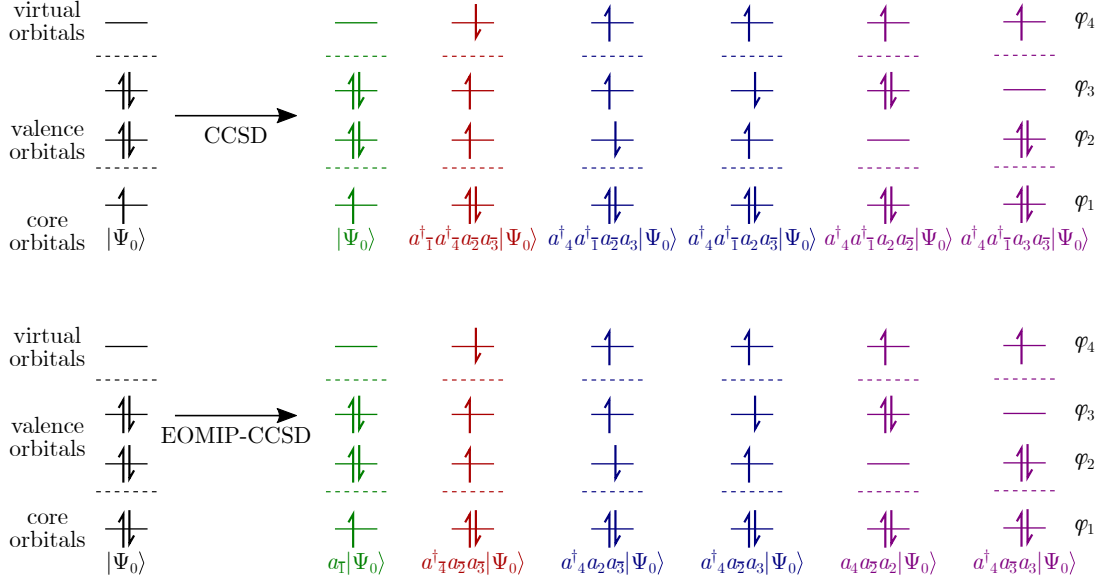


**Figure 1.** Determinants needed to describe Auger decay in a Hilbert space spanned by 4 orbitals as obtained from CCSD (upper part) or EOMIP-CCSD (lower part) calculations. See text for further explanation.

## 2.2. Auger channel projection

In this work, we demonstrate how to gain access to partial decay widths using other complex-variable electronic-structure methods besides CCSD. The new method can be seen as a generalization of the CVS projector [3]. The latter removes from the excitation manifold all determinants where valence electrons are excited into core orbitals, thus all those marked in red, blue and purple in Figure 1. In this way, the decay is quenched and the imaginary part of the energy stays zero apart from contributions resulting from the representation of the wave function in a finite basis set.[2, 28]

The CVS projector can be thought of as a sum of projectors representing individual Auger decay channels, which we will call Auger channel projectors (ACPs). We now determine the wave function under the constraint that only the amplitudes leading to certain Auger final states are zero. Because we would like to keep the wave function as similar as possible to those obtained with or without CVS, we suggest two ways to use this concept to determine partial widths:

In the “in” variant of the ACP, a single Auger decay channel is included in the wave function so that the imaginary part of the energy changes from approximately zero in the CVS method to a negative number. Because the imaginary part of the energy is not necessarily zero in finite basis set calculations with a CVS method, we choose to calculate the partial width as the difference between the imaginary energies obtained with ACP and CVS. The advantage of this “in” variant is that the observed decay can be attributed unequivocally to the active decay channel.

In the “out” variant of the ACP, a single decay channel is removed from the excitation manifold.  $\text{Im}(E)$  will be less negative than with the original method where all decay channels are active. We then evaluate the partial width from the energy difference between the unmodified wave function and the ACP variant with one channel projected out. This carries the benefit that the result is much closer to the wave function that includes all decay channels so that the interaction between different decay processes and its effect on the energy is considered.

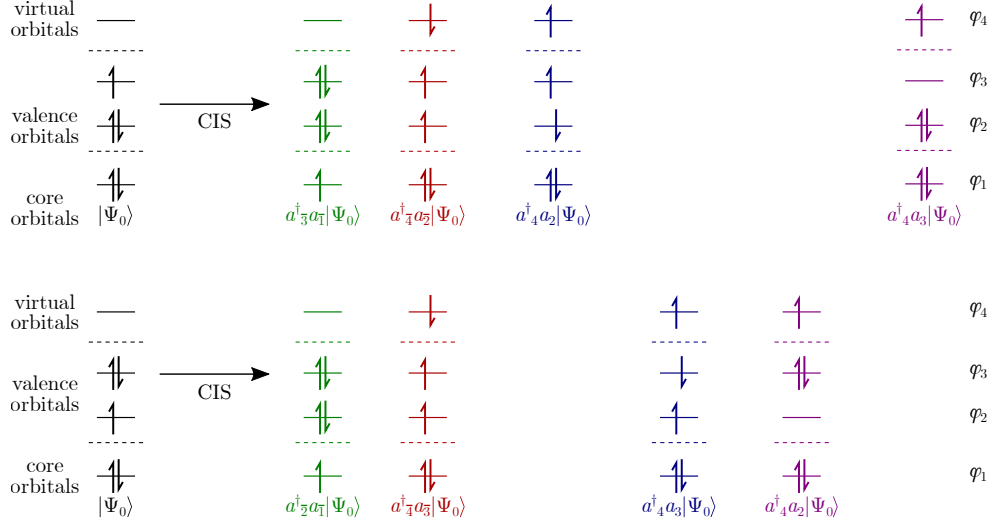


**Figure 2.** Determinants needed to describe Auger decay in a Hilbert space spanned by 4 orbitals as obtained from different CIS calculations. See text for further explanation.

Since the computational cost of a single EOMIP-CCSD calculation scales as  $N_{\text{occ}}^2 N_{\text{virt}}^3$  and since there are in general  $N_{\text{occ}}^2$  decay channels, an ACP-EOMIP-CCSD treatment effectively scales as  $N_{\text{occ}}^4 N_{\text{virt}}^3$  if all decay channels shall be considered individually. The cost of CCSD scales as  $N_{\text{occ}}^2 N_{\text{virt}}^4$  so that ACP-EOMIP-CCSD is, in theory, preferable over decomposition of the CCSD energy in terms of computational cost if  $N_{\text{virt}} > N_{\text{occ}}^2$ . This is the case in typical complex-variable calculations. Also, EOMIP-CCSD can be based on a closed-shell reference state, which requires less memory than an open-shell CCSD treatment of the core-ionized state. We note, however, that our current implementation of ACPs is not able to carry out multiple consecutive EOMIP-CCSD calculations with different ACPs; instead the CCSD calculation for the reference state needs to be repeated.

### 2.3. Application of Auger channel projectors to CIS wave functions

Because it involves two electrons, Auger decay is sometimes referred to as a “correlation-driven” process [44–46]. However, this does not mean that a correlated electronic-structure method needs to be employed for describing it. Namely, it is possible to describe Auger decay with a CIS wave function [47, 48], which only comprises single excitations out of some reference determinant  $|\Psi_0\rangle$ . CIS can be implemented with  $N^4$  scaling and is size-extensive similar to EOM-CC methods and in contrast to higher-order CI methods.

Describing Auger decay with a CIS wave function requires to choose a reference determinant whose single-excitation manifold comprises both the core-ionized determinant and the final state of Auger decay. As illustrated in Figure 2, this is only possible if the reference determinant has a hole in a valence shell and this hole is also present in the Auger final state. This implies that a CIS calculation can only describe a subset and never all possible Auger decay channels. The imaginary part of the CIS energy must therefore not be interpreted as a total Auger decay width.

Figure 2 shows that each decay channel is described by at least one CIS wave function. More specifically, determinants representing closed-shell final states (purple in

Figure 2) are included in only one CIS wave function, whereas the red determinants associated with triplet final states are each contained in exactly two CIS wave functions. Open-shell singlet final states are described by the blue determinants, which are also each contained in exactly one CIS wave function. However, for a proper description of an open-shell singlet, one needs to combine the blue determinants in pairs while this is not needed for the red ones. Also note that the blue determinants do not contribute to the low-spin components of the triplet final states because all determinants in Figure 2 have  $M_S = 1/2$  and the outgoing Auger electron has necessarily alpha spin in the blue determinants.

Even though this analysis is approximate because we start from an unrestricted Hartree-Fock (HF) reference determinant, which is not a spin eigenfunction, it suggests the following procedure to compute the total Auger decay width using CIS: We first construct all possible HF determinants with a hole in a valence orbital and then apply the ACPs as introduced in Sec. 2.2 to the corresponding CIS wave functions to identify the contributions of individual determinants to the decay width. In a second step, we combine the obtained results as follows: Contributions from triplet final states (red determinants in Figure 2) are averaged, while contributions from singlet final states (blue and purple determinants in Figure 2) are simply added up. We add that a straightforward summation of the imaginary energies obtained in the different CIS calculations may offer a good approximation to the total Auger decay width because triplet decay channels typically contribute much less than singlet states.

We also note that there is no unambiguous way to obtain the core-ionization energy from such CIS calculations because the CIS eigenvalues represent only energy differences between the core-ionized state and different valence-ionized states and do not involve the neutral ground state. Furthermore, these energies cannot be expected to be accurate given the limited accuracy of CIS excitation energies in general [48].

#### 2.4. Special considerations for non-Abelian point groups

Molecules with non-Abelian point-group symmetry can possess degenerate occupied orbitals, which complicates the extraction of partial decay widths from complex-variable calculations. We illustrate this in the following for methane ( $\text{CH}_4$ ) which has the electronic configuration  $(1a_1)^2(2a_1)^2(1t_2)^6$ . The analysis applies to CIS, CCSD, and EOMIP-CCSD wave functions alike.

As discussed in Sec. 2.2, it is necessary to set to zero all excitations that describe a particular decay channel in order to calculate the respective partial width. In decay channels where at most one degenerate occupied orbital is involved, these excitations can be identified by considering only the occupancy of the valence orbitals.

For example, for methane every  $(2a_1)^{-2}$  determinant describes decay into the corresponding  $^1A_1$  state. The outgoing Auger electron must occupy a virtual orbital of  $a_1$  symmetry as well because the core-ionized state has  $^2A_1$  symmetry overall but this need not be taken into account for the determination of partial widths. Likewise, every  $(2a_1)^{-1}(1t_2)^{-1}$  determinant contributes to decay into the  $^1T_2$  or  $^3T_2$  state depending on the spin of the outgoing electron. Here, the equivalence of  $(2a_1)^{-1}(2t_2^x)^{-1}$ ,  $(2a_1)^{-1}(2t_2^y)^{-1}$ , and  $(2a_1)^{-1}(2t_2^z)^{-1}$  can be exploited to reduce the number of necessary calculations.

In contrast,  $(1t_2)^{-2}$  determinants contribute to four different decay channels:  $^1A_1$ ,  $^1T_2$ ,  $^1E$ , and  $^3T_1$  according to the direct product  $t_2 \otimes t_2$ . Singlet and triplet channels can be distinguished depending on whether the outgoing electron has  $\alpha$  or  $\beta$  spin, but for the

distinction between the different singlet states it is necessary to consider in addition if the irreducible representation of the virtual orbital where the outgoing electron resides is  $a_1$ ,  $e$ , or  $t_2$ . The partial widths can then be determined by projecting out at once all  $(1t_2)^{-2}$  determinants where virtual orbitals of a particular symmetry have been filled and bearing in mind that the irreducible representation of the core-ionized state is  $A_1$ . We modified our previous implementation [29] according to these thoughts; however, special attention must be paid to the case of CIS. As discussed in Sec. 2.3, CIS calculations need to be based on HF determinants with a hole in a valence shell. If this shell is degenerate in the closed-shell HF wave function, the degeneracy is broken in the corresponding cationic wave function. As a consequence, the degeneracy of virtual shells is also lost so that the identification of the physical decay channels becomes ambiguous.

In this work, we assign the symmetry-broken virtual orbitals that host the Auger electron to the irreducible representations of the molecular point group by energetic proximity: those which are closest to each other are assumed to be degenerate if the electronic wave function transformed to the molecular point group. Consider as a numerical illustration a HF wave function for the methane cation: The artificial splitting in the virtual  $e$  orbitals induced by an asymmetric occupation of the  $1t_2$  orbitals amounts to at most 0.07 a.u., which is considerably lower than the energetic separation between virtual orbitals belonging to different shells. The identification of the decay channels is thus easy. However, this is not always the case, especially not if the virtual orbitals to be distinguished belong to the same irreducible representation as the valence shell with the hole. As an example, in the ammonia cation ( $\text{NH}_3^+$ ) the artificial splittings in the virtual  $e$  orbitals amount to up to 0.5 a.u. which makes a distinction between the  ${}^1E$  and  ${}^1A_1$  decay channels dubious.

### 3. Auger decay of core-ionized water

As a proof of concept, we use the  $1a_1^{-1}$  state of the water molecule, with an electronic configuration of  $(1a_1)^1(2a_1)^2(1b_2)^2(3a_1)^2(1b_1)^2$ . We showed before that Auger decay in this system can be accurately described using a basis where  $s$  and  $p$  shells are taken from the aug-cc-pCV5Z basis set and the shells with higher angular momentum from the aug-cc-pCVTZ basis set. Two complex-scaled  $s$ -,  $p$ -, and  $d$ -shells were added on top at each atom [29]. As the augmentation of the basis set with diffuse shells was found to be of minor importance, we employ the “cc-pCVTZ (5sp) + 2×(spd)” basis set in this work. Additional results using 4 complex-scaled  $s$ ,  $p$  and  $d$  shells are reported in the Supplementary Material. The exponents of the complex-scaled shells are obtained using the strategy published earlier [29] and available from the Supplementary Material. We conducted all calculations using a modified version of the Q-Chem program package [49]. The CIS calculations were performed with the complex-variable CCSD and EOM-CCSD codes of Q-Chem [36, 50–53] where we set to zero all CCSD amplitudes and the EOM-CCSD doubles amplitudes.

#### 3.1. CCSD and EOMIP-CCSD results

The total decay half-width of water, calculated as the difference between the imaginary energies of the ground state and the core-ionized state, amounts to 71 meV with EOMIP-CCSD at  $\theta_{\text{opt}} = 22^\circ$  and 70 meV with  $\Delta\text{CCSD}$  at  $\theta_{\text{opt}} = 16^\circ$ . Partial half-widths obtained using the energy decomposition method introduced in our earlier

**Table 1.** Partial decay half-widths of core-ionized water calculated with CCSD and EOMIP-CCSD using the cc-pCVTZ (5sp) basis set with 2 complex scaled s-, p- and d-shells on each atom. All values in meV.

Decay channel	EOM-CCSD	CCSD	EOMIP-CCSD	ACP-CCSD		ACP-EOMIP-CCSD	
	Fano <sup>a</sup>		decomposition	“out”	“in”	“out”	“in”
2a <sub>1</sub> 2a <sub>1</sub>	7.7	9.1	8.1	9.8	8.9	8.5	8.4
2a <sub>1</sub> 3a <sub>1</sub> (singlet)	6.8	6.8	2.3	6.6	6.7	6.6	6.3
2a <sub>1</sub> 3a <sub>1</sub> (triplet)	1.9	1.3	3.4	1.3	0.9	1.2	1.0
2a <sub>1</sub> 1b <sub>1</sub> (singlet)	4.8	6.5	-3.7	6.0	5.4	6.1	5.9
2a <sub>1</sub> 1b <sub>1</sub> (triplet)	2.1	1.6	2.4	1.5	1.1	1.4	1.2
2a <sub>1</sub> 1b <sub>2</sub> (singlet)	3.2	4.1	3.5	3.8	3.2	4.2	3.9
2a <sub>1</sub> 1b <sub>2</sub> (triplet)	1.5	1.0	3.1	1.1	0.7	1.0	0.8
3a <sub>1</sub> 3a <sub>1</sub>	4.5	5.9	15.1	5.1	5.0	4.6	4.7
3a <sub>1</sub> 1b <sub>1</sub> (singlet)	6.4	8.3	23.2	7.3	7.1	6.9	6.8
3a <sub>1</sub> 1b <sub>1</sub> (triplet)	0.3	0.1	0.2	0.1	0.1	0.1	0.1
3a <sub>1</sub> 1b <sub>2</sub> (singlet)	4.8	8.3	22.4	7.2	6.9	6.1	6.0
3a <sub>1</sub> 1b <sub>2</sub> (triplet)	0.2	0.1	0.2	0.1	0.1	0.1	0.1
1b <sub>1</sub> 1b <sub>1</sub>	6.7	8.1	20.7	7.1	7.1	6.4	6.5
1b <sub>1</sub> 1b <sub>2</sub> (singlet)	5.4	6.9	21.5	6.0	5.9	5.8	5.8
1b <sub>1</sub> 1b <sub>2</sub> (triplet)	0.0	0.0	0.0	0.0	0.0	0.0	0.0
1b <sub>2</sub> 1b <sub>2</sub>	3.6	5.0	14.2	4.3	4.1	3.9	3.8
Sum	59.9	73.1	136.7	67.3	62.4	62.8	61.1

<sup>a</sup> From reference [26].

work [29] are shown in columns 3 and 4 of Table 1. These results illustrate that energy decomposition works only for CCSD but not for EOM-CCSD; the reasons were discussed in Ref. [29].

In contrast, the Auger channel projectors introduced in Sec. 2.2 work for both, CCSD and EOMIP-CCSD. Results obtained with the “in” and “out” versions are shown in the last four columns of Table 1, they are very similar to those obtained by decomposition of the CCSD energy and in qualitative agreement with values obtained using the Feshbach-Fano method [25, 26]. The root mean square (RMS) deviations with respect to the former results vary from 0.4 meV (“out”-ACP-CCSD) to 1.0 (“in”-ACP-EOMIP-CCSD) meV. We add that all ACP calculations were performed at the  $\theta_{\text{opt}}$  of the respective unmodified method; we did not explore the impact of optimizing  $\theta$  for each channel.

The results from Table 1 validate the ACP approach. The “in” and “out” approaches give almost identical values, the RMS deviations between them are only 0.4 meV (CCSD) and 0.16 meV (EOMIP-CCSD), respectively, where the “out” method typically yields partial widths closer to the energy decomposition approach. The largest deviations from energy decomposition occur in the high-energy singlet channels (1b<sub>1</sub>1b<sub>1</sub>, 3a<sub>1</sub>1b<sub>1</sub>, and 3a<sub>1</sub>1b<sub>1</sub>) where ACPs yield partial half-widths that are lower by about 1 meV. Overall, the differences between ACPs and energy decomposition are even smaller. In fact, the comparison with partial widths of H<sub>2</sub>O reported in our previous work [29] shows that adding diffuse functions or changing details of the energy decomposition procedure make a larger impact.

### 3.2. CIS results

As discussed in Sec. 2.3, one needs to perform multiple separate CIS calculations to consider all decay channels. In the case of H<sub>2</sub>O, they are based on four different cationic HF references (2a<sub>1</sub><sup>-1</sup>, 1b<sub>2</sub><sup>-1</sup>, 3a<sub>1</sub><sup>-1</sup>, 1b<sub>1</sub><sup>-1</sup>) where we used the maximum overlap method [54] to ensure convergence to the right state.

To determine the optimal value of the scaling angle  $\theta$ , we considered two different



**Table 2.** Partial decay half-widths of core-ionized water calculated with CIS using different reference determinants and the “out” version of ACPs. The cc-pCVTZ (5sp) basis set with 2 complex scaled s-, p- and d-shells on each atom and a uniform  $\theta = 28^\circ$  are used. Results from the decomposition of the CCSD energy (taken from Table 1) are given as well. All values in meV.

Decay channel	CIS				Total	CCSD
	$2a_1^{-1}$	$1b_2^{-1}$	$3a_1^{-1}$	$1b_1^{-1}$		
$2a_1 2a_1$	8.9	–	–	–	8.9	9.1
$2a_1 3a_1$ (singlet)	4.8	–	2.4	–	7.2	6.8
$2a_1 3a_1$ (triplet)	1.0	–	1.7	–	1.4	1.3
$2a_1 1b_1$ (singlet)	4.5	–	–	1.9	6.4	6.5
$2a_1 1b_1$ (triplet)	1.2	–	–	1.9	1.5	1.6
$2a_1 1b_2$ (singlet)	2.9	1.6	–	–	4.5	4.1
$2a_1 1b_2$ (triplet)	0.7	1.6	–	–	1.2	1.0
$3a_1 3a_1$	–	–	5.7	–	5.7	5.9
$3a_1 1b_1$ (singlet)	–	–	4.2	3.7	7.9	8.3
$3a_1 1b_1$ (triplet)	–	–	0.1	0.2	0.2	0.1
$3a_1 1b_2$ (singlet)	–	3.3	3.3	–	6.6	8.3
$3a_1 1b_2$ (triplet)	–	0.2	0.1	–	0.1	0.1
$1b_1 1b_1$	–	–	–	7.6	7.6	8.1
$1b_1 1b_2$ (singlet)	–	3.7	–	3.2	6.9	6.9
$1b_1 1b_2$ (triplet)	–	0.0	–	0.0	0.0	0.0
$1b_2 1b_2$	–	4.3	–	–	4.3	5.0
Sum	24.0	14.5	18.6	17.5	70.5	73.1
$-\text{Im}(E)$	24.8	16.2	18.1	18.4	77.5	70.X

strategies. A straightforward procedure is to determine separate values for  $\theta$  for each of the four CIS wave functions by minimizing  $|dE_{\text{CIS}}/d\theta|$ . In the present case, this results in values between  $14$  and  $28^\circ$ . However, our ACP-CCSD and ACP-EOMIP-CCSD results (see Sec. 3.1) suggest that it is not necessary to use a different  $\theta$  for each wave function. The partial widths of all decay channels are determined at the same  $\theta$  in these calculations and still sum up to an accurate total width. This is why we additionally used the sum  $\sum_{i=1}^4 |dE_{\text{CIS}}^i/d\theta|$  as criterion to find a uniform  $\theta$  for all calculations. This yields  $\theta_{\text{opt}} = 28^\circ$ ; at this value each trajectory exhibits a local minimum in  $|dE_{\text{CIS}}/d\theta|$ , which is, however, not always the global minimum. One may speculate that the occurrence of multiple minima in  $|dE_{\text{CIS}}/d\theta|$  is an artifact stemming from the unphysical restriction of the configuration space.

Our calculations show that the numerical differences between these two procedures are very small. In the following, we concentrate on the results obtained using a uniform  $\theta$ , whereas results obtained with a separate  $\theta$  for each CIS calculation are available in the Supplementary Material.

The last row of Table 2 shows that the imaginary parts of the CIS energies of the core-ionized states vary between 16 meV and 25 meV and are thus much lower than the CCSD value (70 meV). This is a consequence of the fact that each of the four CIS wave functions contains only a subset of the decay channels present in the CCSD wave function. The simplest way to solve this problem is to add up the  $\text{Im}(E)$  values from the four CIS calculations, which results in a total half-width of 77.5 meV, that is, the deviation from CCSD is ca. 10%. As discussed in Sec. 2.3, this simple summation counts the triplet channels twice. This is confirmed by adding up the CCSD partial widths (last column of Table 2) and doubling the widths of the triplet channels, which results in 77.2 meV.

The double counting of triplet channels is avoided by computing partial decay widths using ACPs and then summing over the singlet channels while averaging the values for the triplet channels as discussed in Sec. 2.3. In Table 2, we report the partial widths

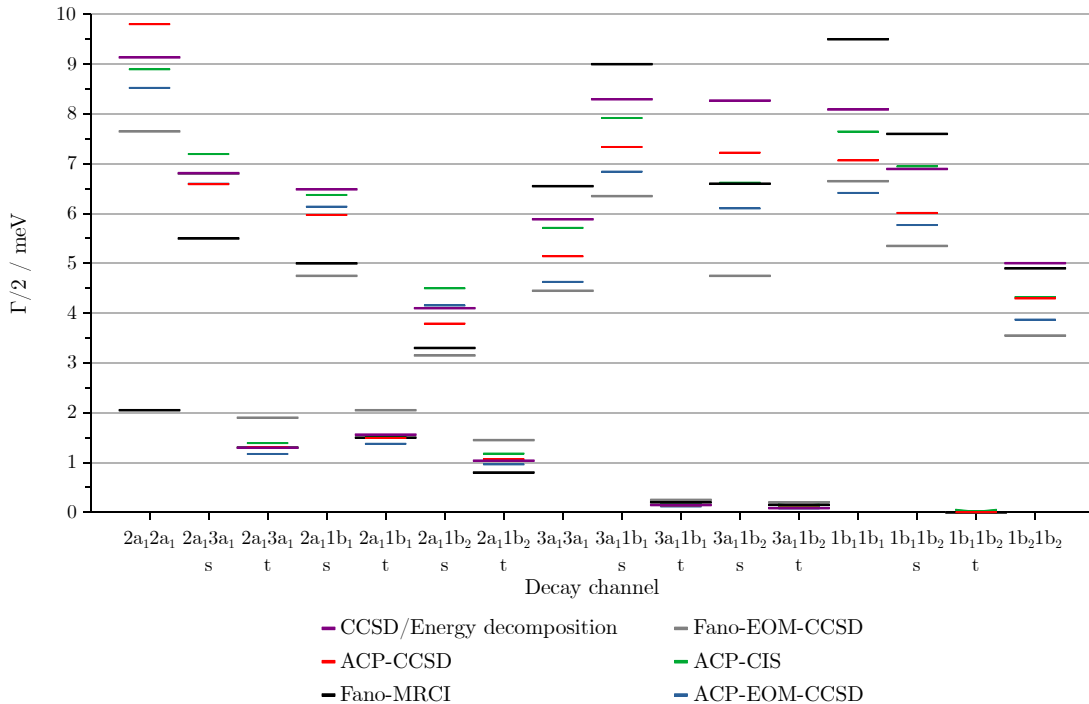


**Figure 3.** Partial decay widths of core-ionized water computed with different methods. Complex-variable calculations are done with the cc-pCVTZ (5sp) basis set with 2 complex scaled s-, p- and d-shells on each atom; all values are available from Tables 1 and 2. Fano-MRCI and Fano-EOM-CCSD results are taken from Refs. [24, 55] and [26], respectively.

obtained with “out”-ACPs, while results computed with “in”-ACPs are available in the Supplementary Material. Our results demonstrate that ACP-CIS produces partial widths in remarkable agreement with those from the decomposition of the CCSD energy, the RMS deviation amounts to only 0.5 meV. The largest deviation between ACP-CIS and CCSD (1.7 meV) occurs for the  $3a_11b_2$  singlet channel, for all other channels it stays below 1 meV. Recombining the partial widths to a total decay half-width results in 70.5 meV, which is very close to the numbers obtained with  $\Delta$ CCSD (70 meV) and EOMIP-CCSD (71 meV).

This good agreement of CIS with CCSD and EOMIP-CCSD demonstrates that the individual decay channels are, in general, well described by CIS. The representation of a channel by a single configuration according to Figure 2 appears to be a valid approximation. However, there are a few decay channels where this may not be the case. This is apparent from Figure 3 where results from different methods for the partial widths of core-ionized water are compared. Even though the overall agreement between all methods is good, there are a few conspicuous cases where Fano-MRCI deviates from all other results, in particular  $2a_12a_1$  and to a lesser degree  $2a_13a_1$  and  $1b_11b_1$ . This may indicate that these channels are not so well described by a single configuration, which may be captured better by MRCI.

#### 4. Further applications: Ne, NH<sub>3</sub>, and CH<sub>4</sub>

As further applications of ACPs, we investigated Auger decay of core-ionized states of methane (CH<sub>4</sub>), ammonia (NH<sub>3</sub>) and the neon atom. Like H<sub>2</sub>O, all these species have

10 electrons in their neutral ground state. The same basis sets as in Sec. 3 are used, details are available from the Supplementary Material.

#### 4.1. Total decay widths

Our results for total half-widths are summarized in Table 3. For CIS, “out”-ACPs and a uniform  $\theta_{\text{opt}}$  were used as discussed in Sec. 3.2. Additional results including  $\theta_{\text{opt}}$  values, CIS results with “in”-ACPs, and CIS contributions from individual calculations can be found in the Supplementary Material.

The different methods yield very similar decay half-widths for all species: no deviation larger than 5 meV is observed. Our results are also in qualitative agreement with experimental values [56–61] and with decay widths computed using Fano’s theory [26]. In particular, EOMIP-CCSD,  $\Delta$ CCSD, and CIS all produce the correct dependence of the Auger decay width on the nuclear charge  $Z$ , that is, higher  $Z$  leads to faster decay. This trend is well-known and has been related to the higher kinetic energy of the Auger electron due to higher  $Z$  [1, 62, 63].

We add that there is disagreement between different experiments about the Auger decay width of methane [58–61] with values for the half-width ranging from 41 to 60 meV. Our results as well as Fano’s theory are more in line with the lower values, but the results for the other species also suggest that our methods and Fano’s theory both may underestimate the decay width systematically. This disagreement with experimental values may be caused by processes involving more than two electrons, which are not described by any of our methods. However, it may also be ascribed in part to the basis set. Notably, we employed in our previous work [29] the “aug-cc-pCVTZ (5sp) + 2×(spd)” basis set (instead of “cc-pCVTZ (5sp) + 2×(spd)” here) and obtained values of 75 and 78 meV for the total half-width of H<sub>2</sub>O using EOMIP-CCSD and  $\Delta$ CCSD, respectively. Also, while 2 complex-scaled s, p, and d-shells are sufficient for H<sub>2</sub>O, 4 of them appear to be necessary for the neon atom. These differences are documented in the Supplementary Material.

**Table 3.** Total decay half-widths in meV of the core-ionized neon atom and the water, ammonia, and methane molecules.

Method	Ne	H <sub>2</sub> O	NH <sub>3</sub>	CH <sub>4</sub>
EOMIP-CCSD <sup>a</sup>	110	71	56	37
$\Delta$ CCSD <sup>a</sup>	115	70	55	38
CIS <sup>b</sup>	113	71	53	37
Fano-EOM-CCSD <sup>c</sup>	109	61	–	33
Experiment <sup>d</sup>	129	80	–	47

<sup>a</sup> This work. Computed with the cc-pCVTZ (5sp) + 2×(spd) basis set [Ne: 4×(spd)] and evaluated as imaginary part of the total energy.

<sup>b</sup> This work. Computed with the cc-pCVTZ (5sp) + 2×(spd) basis set [Ne: 4×(spd)] and “out”-ACPs, evaluated as weighted sum of partial widths, see Sec. 2.3 for details.

<sup>c</sup> From Ref. [26]. Computed using Coulomb waves for the Auger electron. For H<sub>2</sub>O and CH<sub>4</sub>, values of  $Z_{\text{eff}}$  of 4.9 (H<sub>2</sub>O) and 3.6 (CH<sub>4</sub>) were assumed for all channels, while for Ne, different values were assumed for each channel.

<sup>d</sup> From Refs. [56] (Ne), [57] (H<sub>2</sub>O), and [58] (CH<sub>4</sub>).

## 4.2. Partial decay widths

Partial decay half-widths for Ne, NH<sub>3</sub>, and CH<sub>4</sub> are available from Tables 4, 5, and 6, respectively. Further results and a graphical comparison of different methods are available from the Supplementary Material. In line with previous results [29], we observe that partial widths and branching ratios are significantly more sensitive towards the computational details than total widths. Details are discussed in the following.

**Table 4.** Partial decay half-widths of core-ionized neon in meV.

Decay channel	CCSD	EOMIP-CCSD out-ACP	CIS	CCSD energy decomp.	EOM-CCSD Fano <sup>a</sup>	expt. <sup>b</sup>
<sup>1</sup> D (2p <sup>-2</sup> )	69.4	63.7	68.0	75.5	58.8	78.2(21)
<sup>1</sup> P (2s <sup>-1</sup> 2p <sup>-1</sup> )	28.1	25.8	23.0	29.6	19.6	22.1(7)
<sup>3</sup> P (2s <sup>-1</sup> 2p <sup>-1</sup> )	6.9	5.6	5.4	6.7	11.9	8.1(3)
<sup>1</sup> S (2p <sup>-2</sup> )	4.9	4.5	3.1	5.7	13.6	7.9(3)
<sup>1</sup> S (2s <sup>-2</sup> )	13.8	12.3	13.3	13.5	5.3	12.2(4)

<sup>a</sup> From reference [26].

<sup>b</sup> From reference [56].

The core-ionized neon atom with the electronic configuration of (1s)<sup>1</sup>(2s)<sup>2</sup>(2p)<sup>6</sup> has 5 main decay channels. Their relative importance is captured correctly by all methods: the <sup>1</sup>D channel is broadest followed by the <sup>1</sup>P channel. Table 4 shows that the ACP methods tend to produce systematically smaller widths for all channels than the decomposition of the CCSD energy. This tendency is also present for H<sub>2</sub>O (Sec. 3.1, Tab. 1), but it is a lot more pronounced for the <sup>1</sup>D and <sup>1</sup>P channels of Ne. For the <sup>1</sup>D channel, it leads to the ACP methods underestimating the experimental width by 10–20%, while CCSD energy decomposition agrees within 3% with the experiment. However, for the next-broadest channel (<sup>1</sup>P) the performance is reversed and ACP-CIS is closest to the experimental value. Notably, the <sup>1</sup>D and <sup>1</sup>P channels are also most sensitive to the complex-scaled basis set. As shown in the Supplementary Material, the respective branching ratio is significantly distorted when only 2 instead of 4 complex-scaled shells are employed, while all remaining channels, which are narrower, are less sensitive.

**Table 5.** Partial decay half-widths of core-ionized ammonia in meV.

Decay channel	CCSD	EOMIP-CCSD out-ACP	CIS	CCSD energy decomp.
<sup>1</sup> A <sub>1</sub> (2a <sub>1</sub> <sup>-2</sup> )	7.8	7.2	7.6	7.3
<sup>1</sup> E (2a <sub>1</sub> <sup>-1</sup> 1e <sup>-1</sup> )	7.2	7.7	7.7	7.9
<sup>3</sup> E (2a <sub>1</sub> <sup>-1</sup> 1e <sup>-1</sup> )	2.0	1.7	2.1	2.0
<sup>1</sup> A <sub>1</sub> (1e <sup>-2</sup> )	2.6	2.5	1.9	3.2
<sup>1</sup> E (1e <sup>-2</sup> )	10.2	8.3	9.5	12.1
<sup>3</sup> A <sub>2</sub> (1e <sup>-2</sup> )	0.0	0.0	0.0	0.0
<sup>1</sup> A <sub>1</sub> (3a <sub>1</sub> <sup>-2</sup> )	5.8	4.8	5.8	6.7
<sup>1</sup> A <sub>1</sub> (2a <sub>1</sub> <sup>-1</sup> 3a <sub>1</sub> <sup>-1</sup> )	5.2	5.3	5.6	5.3
<sup>3</sup> A <sub>1</sub> (2a <sub>1</sub> <sup>-1</sup> 3a <sub>1</sub> <sup>-1</sup> )	1.1	1.0	1.1	1.1
<sup>1</sup> E (3a <sub>1</sub> <sup>-1</sup> 1e <sup>-1</sup> )	12.2	10.3	11.5	14.2
<sup>3</sup> E (3a <sub>1</sub> <sup>-1</sup> 1e <sup>-1</sup> )	0.1	0.1	0.2	0.1

The core-ionized ammonia molecule with the electronic configuration (1a<sub>1</sub>)<sup>1</sup>(2a<sub>1</sub>)<sup>2</sup>(1e)<sup>4</sup>(3a<sub>1</sub>)<sup>2</sup> has 11 main decay channels. As Table 5 illustrates, all our methods agree that two <sup>1</sup>E channels (1e<sup>-2</sup> and 3a<sub>1</sub><sup>-1</sup>1e<sup>-1</sup>) are broadest followed by a third <sup>1</sup>E channel (2a<sub>1</sub><sup>-1</sup>1e<sup>-1</sup>) and a <sup>1</sup>A<sub>1</sub> channel (2a<sub>1</sub><sup>-2</sup>). This overall consistency between the methods is also reflected by the good agreement in the total width

**Table 6.** Partial decay half-widths of core-ionized methane in meV.

Decay channel	CCSD	EOMIP-CCSD out-ACP	CIS	CCSD energy decomp.	EOM-CCSD Fano <sup>a</sup>
$^1A_1 (2a_1^{-2})$	5.8	5.9	5.7	5.9	6.6
$^1T_2 (2a_1^{-1}1t_2^{-1})$	8.7	7.1	9.5	8.6	7.1
$^3T_2 (2a_1^{-1}1t_2^{-1})$	2.3	2.4	2.9	2.9	3.4
$^1T_2 (1t_2^{-2})$	12.0	14.0	19.3	16.3	8.0
$^1A_1 (1t_2^{-2})$	1.1	1.1	1.3	0.9	3.0
$^1E (1t_2^{-2})$	6.5	6.3	9.9	8.3	5.4
$^3T_1 (1t_2^{-2})$	0.0	0.1	0.0	0.0	0.0

<sup>a</sup> From Ref. [26].

(Tab. 3). Especially remarkable is the good performance of CIS because these calculations are based on symmetry-broken HF determinants and the identification of the decay channels is dubious in this case as we discussed in Sec. 2.4. From Tab. 5, it is also apparent that, similar to neon, all ACP methods yield smaller widths than energy decomposition on average. This is most pronounced for the two broadest  $^1E$  channels. Together with the fact that EOMIP-CCSD yields somewhat smaller widths than CCSD for some channels, significantly different branching ratios can be obtained from the different methods in some cases.

The core-ionized methane molecule with the electronic configuration  $(1a_1)^1(2a_1)^2(2t_2)^6$  features 7 decay channels. Table 6 shows that all our methods as well as Fano-EOM-CCSD agree that the  $^1T_2 (1t_2^{-2})$  channel is broadest but apart from this there is substantial disagreement between the methods about most singlet channels. While there are some channels with small deviations, in particular  $^1A_1 (2a_1^{-2})$ ,  $^1T_2 (2a_1^{-1}1t_2^{-1})$ , and  $^1A_1 (1t_2^{-2})$ , the widths of the  $^1E$  channels and the other  $^1T_2$  channels differ substantially between the methods. On average, decomposition of the CCSD energy yields the largest partial widths for  $CH_4$ , whereas Fano-EOM-CCSD yields the smallest widths with the ACP results falling in between. The same trend as for  $H_2O$ ,  $Ne$ , and  $NH_3$  is thus observed; it is, however, more pronounced for  $CH_4$  and  $Ne$  than for  $NH_3$  and  $H_2O$ .

Taking a step back and comparing the different species ( $H_2O$ ,  $NH_3$ ,  $CH_4$  and  $Ne$ ), we observe that the agreement between ACPs, energy decomposition, and Fano’s theory is best for totally symmetric decay channels, whereas substantial differences occur for other channels, especially for decay into degenerate final states. For  $H_2O$ , there are no degenerate states so that the agreement is much better than for the other species. A detailed investigation of this phenomenon is beyond the present work, but based on the good agreement with experimental values for neon, we think that the energy decomposition approach gives the best results. This would mean that removing certain decay channels from the excitation manifold as done in the “out”-ACP approach works better if these channels are totally symmetric. We reiterate the different basis-set dependence of  $H_2O$  and  $Ne$  in this context: While using 2 instead of 4 complex-scaled shells makes little impact on all  $H_2O$  results, the width of the  $^1D$  channel of  $Ne$  changes considerably.

### 4.3. Inner-valence and outer-valence orbitals

While it is well known that the total Auger decay width of a core hole increases with nuclear charge  $Z$  [1, 62, 63], trends in partial widths are more involved. To compare partial widths between  $CH_4$ ,  $NH_3$ ,  $H_2O$ , and  $Ne$ , we distinguish inner-valence and

outer-valence orbitals: The  $2a_1$  orbitals in water, ammonia, and methane and the  $2s$  orbital in neon are defined as inner-valence, while all other higher-lying orbitals are defined as outer-valence. This distinction is useful because holes in inner-valence and outer-valence orbitals relax in different ways. In particular, only inner-valence holes can undergo ICD [34, 64], whereas outer-valence holes do not have enough energy. Partial Auger decay widths involving inner-valence orbitals thus influence ICD rates.

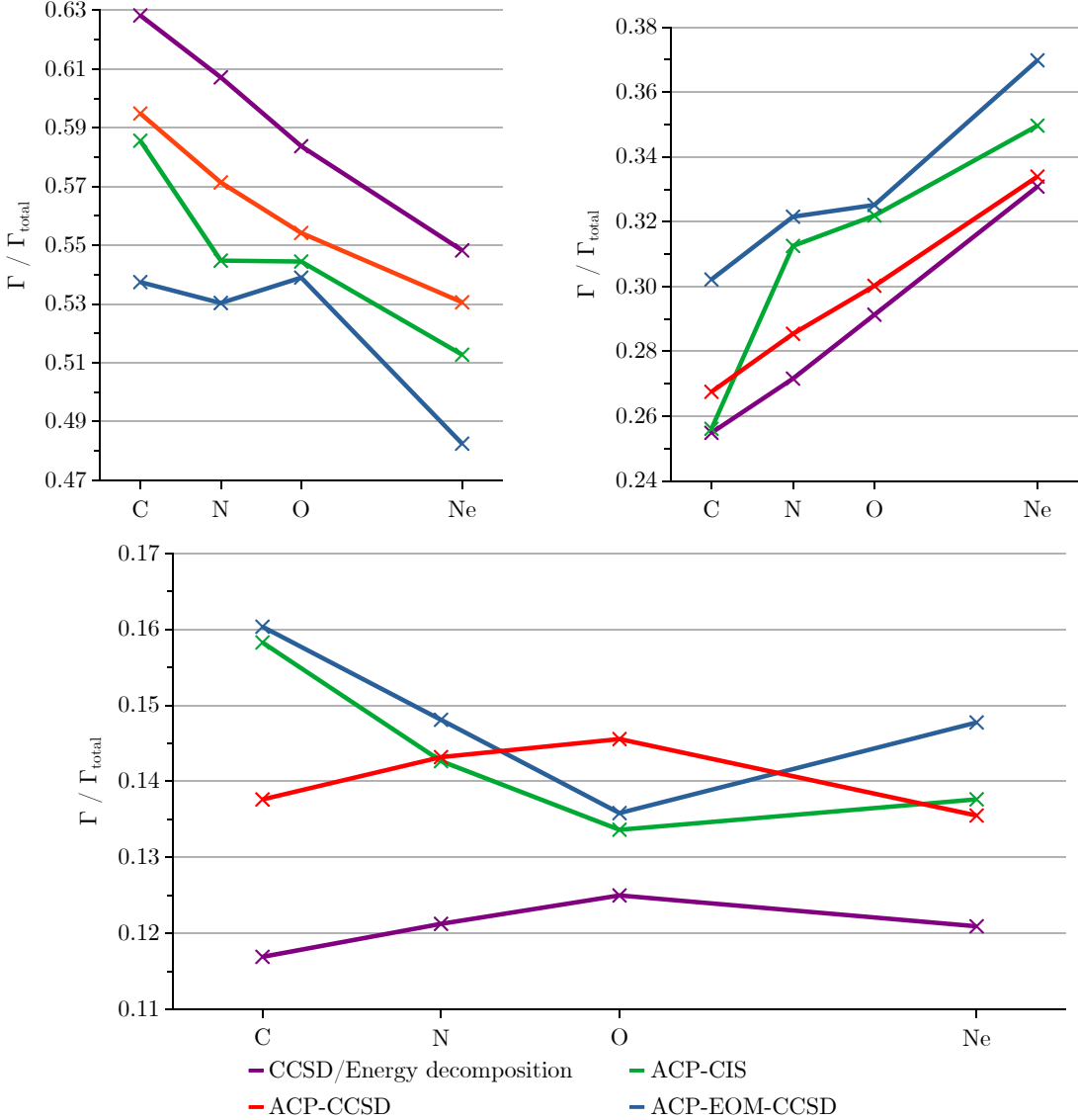


**Figure 4.** Relative contributions of decay channels involving two outer-valence spin-orbitals (upper left), two inner-valence spin-orbitals (bottom), and one outer-valence and one inner-valence spin-orbital (upper right) to the total Auger decay width of  $\text{CH}_4$ ,  $\text{NH}_3$ ,  $\text{H}_2\text{O}$ , and  $\text{Ne}$ .

For all systems investigated here, there are 2 inner-valence spin-orbitals and 6 outer-valence spin-orbitals. From statistical considerations, one would thus expect the pure inner-valence channel to contribute  $1/16 \approx 6\%$  to the total decay width. Figure 4 shows that this is not the case, the inner-valence decay channel rather contributes 12–16% depending on the system and method. Furthermore, Figure 4 demonstrates that the relative contribution of decay channels involving two outer-valence spin-orbitals

decreases with growing  $Z$ . In return, decay involving one inner-valence and one outer-valence spin-orbital becomes more important, while the contribution of the pure inner-valence channel depends only weakly on  $Z$ . All our methods agree on these trends, although there is a minor disagreement about the channel involving two inner-valence spin-orbitals: CIS and EOMIP-CCSD find the highest relative contribution of this channel for  $\text{H}_2\text{O}$  where CCSD finds the lowest contribution. In sum, our results indicate that ICD and related processes that require inner-valence holes are more likely to occur after Auger decay in neon than in molecules with lighter nuclei.

## 5. Conclusions and Outlook

We have introduced Auger channel projectors (ACPs) for the determination of partial Auger decay widths from complex-variable electronic-structure calculations. ACPs are related to the projectors used for implementing the core-valence separation but specific to particular decay channels.

While we showed previously that partial Auger decay widths can be computed by decomposing the imaginary part of the CCSD energy [29], the ACP approach can be combined with EOMIP-CCSD and CIS as well. Results from both approaches are generally in good agreement although widths for decay into degenerate states of molecules with high symmetry appear to be systematically underestimated by ACP methods. A further advantage of the energy decomposition approach is that it is always based on a single CCSD calculation irrespective of the number of decay channels, whereas the ACP approaches require to determine the wave function anew for each decay channel. On the other hand, because EOMIP-CCSD is less costly than CCSD, ACP-EOMIP-CCSD is potentially computationally cheaper than CCSD energy decomposition. Moreover, the EOMIP-CCSD wave function is a spin eigenfunction and there is no need to solve the HF and CCSD equations for the core-vacant state, which can be problematic.

Also, we showed that accurate total and partial Auger decay widths can be computed with ACPs applied to CIS wave functions although an individual CIS wave function describes only a subset of the decay channels. While CIS is attractive in terms of computational cost, the main drawback of its application to Auger decay is that this requires to determine the HF wave functions of all states with a hole in a valence shell. This may be impractical for larger molecules and may also be affected by convergence problems.

We conclude by remarking that ACPs are not only useful for modeling Auger decay, but can be applied to resonant Auger decay as well as decay processes that do not involve core orbitals such as ICD.

## Acknowledgements

F.M. thanks Garrette Pauley Paran, Anthuan Ferino Pérez, Valentina Parravicini, and Jonas Nijssen for helpful discussions about point-group symmetry and for help in verifying the implementation. T.-C. J. gratefully acknowledges funding from the European Research Council (ERC) under the European Union’s Horizon 2020 research and innovation program (Grant Agreement No. 851766). F. M. is grateful for a Kekulé fellowship (K 208/24) by the Fonds der Chemischen Industrie.

## References

- [1] Agarwal, B. K., *X-ray spectroscopy: an introduction* (Springer, 2013).
- [2] Jagau, T.-C., “Theory of electronic resonances: fundamental aspects and recent advances”, *Chem. Comm.* **58**, 5205–5224 (2022).
- [3] Cederbaum, L. S., Domcke, W., and Schirmer, J., “Many-body theory of core holes”, *Phys. Rev. A* **22**, 206–222 (1980).
- [4] Wenzel, J., Wormit, M., and Dreuw, A., “Calculating core-level excitations and X-ray absorption spectra of medium-sized closed-shell molecules with the algebraic-diagrammatic construction scheme for the polarization propagator”, *J. Comput. Chem.* **35**, 1900 (2014).
- [5] Wenzel, J., Wormit, M., and Dreuw, A., “Calculating X-ray absorption spectra of open-shell molecules with the unrestricted algebraic-diagrammatic construction scheme for the polarization propagator”, *J. Chem. Theory Comput.* **10**, 4583 (2014).
- [6] Zheng, X. and Cheng, L., “Performance of delta-coupled-cluster methods for calculations of core-ionization energies of first-row elements”, *J. Chem. Theory Comput.* **15**, 4945–4955 (2019).
- [7] Coriani, S. and Koch, H., “Communication: X-ray absorption spectra and core-ionization potentials within a core-valence separated coupled cluster framework”, *J. Chem. Phys.* **143**, 181103 (2015).
- [8] Vidal, M. L., Feng, X., Epifanovsky, E., Krylov, A. I., and Coriani, S., “New and efficient equation-of-motion coupled-cluster framework for core-excited and core-ionized states”, *J. Chem. Theory Comput.* **15**, 3117–3133 (2019).
- [9] Liu, J., Matthews, D., Coriani, S., and Cheng, L., “Benchmark calculations of K-edge ionization energies for first-row elements using scalar-relativistic core-valence-separated equation-of-motion coupled-cluster methods”, *J. Chem. Theory Comput.* **15**, 1642–1651 (2019).
- [10] Tennyson, J., “Electron-molecule collision calculations using the R-matrix method”, *Phys. Rep.* **491**, 29–76 (2010).
- [11] Gorczyca, T. W., “Auger decay of the photoexcited  $1s^{-1}np$  Rydberg series in neon”, *Phys. Rev. A* **61**, 024702 (2000).
- [12] García, J., Kallman, T. R., Witthoef, M., Behar, E., Mendoza, C., Palmeri, P., Quinet, P., Bautista, M. A., and Klapisch, M., “Nitrogen K-shell photoabsorption”, *Astrophys. J. Suppl. S.* **185**, 477–485 (2009).
- [13] Fano, U., “Effects of configuration interaction on intensities and phase shifts”, *Phys. Rev.* **124**, 1866–1878 (1961).
- [14] Feshbach, H., “A unified theory of nuclear reactions. II,” *Ann. Phys. (N.Y.)* **19**, 287–313 (1962).
- [15] Langhoff, P. W. and Corcoran, C. T., “Stieltjes imaging of photoabsorption and dispersion profiles”, *J. Chem. Phys.* **61**, 146–159 (1974).
- [16] Carravetta, V. and Ågren, H., “Stieltjes imaging for molecular Auger transition rates: Application to the Auger spectrum of water”, *Phys. Rev. A* **35**, 1022–1032 (1987).
- [17] Averbukh, V. and Cederbaum, L. S., “Ab initio calculation of interatomic decay rates by a combination of the Fano ansatz, Green’s-function methods, and the Stieltjes imaging technique”, *J. Chem. Phys.* **123**, 204107 (2005).
- [18] Kolorenč, P. and V. Averbukh, “Fano-ADC(2,2) method for electronic decay rates”, *J. Chem. Phys.* **152**, 214107 (2020).
- [19] Kolorenč, P. and Averbukh, V., “K-shell Auger lifetime variation in doubly ionized Ne and first row hydrides”, *J. Chem. Phys.* **135**, 134314 (2011).
- [20] Ellison, F. O., “Theoretical equations for photoionization cross sections of polyatomic molecules in plane-wave and orthogonalized plane-wave approximations”, *J. Chem. Phys.* **61**, 507 (1974).
- [21] Colle, R., Simonucci, S. and Woodruff, T. O., “Auger emissions from the LiF molecule: Calculation of probabilities and energies”, *Phys. Rev. A* **38**, 694 (1988).
- [22] Zähringer, K., Meyer, H.-D., and Cederbaum, L. S., “Molecular scattering wave functions



- for Auger decay rates: The Auger spectrum of hydrogen fluoride”, *Phys. Rev. A* **45**, 5643–5652 (1992).
- [23] Yarzhevsky, V. G. and Sgamellotti, A., “Auger rates of second-row atoms calculated by many-body perturbation theory”, *J. Electron Spectrosc. Relat. Phenom.* **125**, 13–24 (2002).
- [24] Inhester, L., Burmeister, C. F., Groenhof, G., and Grubmüller, H., “Auger spectrum of a water molecule after single and double core ionization”, *J. Chem. Phys.* **136**, 144304 (2012).
- [25] Skomorowski, W. and Krylov, A. I., “Feshbach–Fano approach for calculation of Auger decay rates using equation-of-motion coupled-cluster wave functions. I. Theory and implementation”, *J. Chem. Phys.* **154**, 084124 (2021).
- [26] Skomorowski, W. and Krylov, A. I., “Feshbach–Fano approach for calculation of Auger decay rates using equation-of-motion coupled-cluster wave functions. II. Numerical examples and benchmarks”, *J. Chem. Phys.* **154**, 084125 (2021).
- [27] Moiseyev, N., *Non-Hermitian Quantum Mechanics* (Cambridge University Press, 2011).
- [28] Jagau, T.-C., Bravaya, K. B., and Krylov, A. I., “Extending quantum chemistry of bound states to electronic resonances”, *Annu. Rev. Phys. Chem.* **68**, 525–553 (2017).
- [29] Matz, F. and Jagau, T.-C., “Molecular Auger decay rates from complex-variable coupled-cluster theory”, *J. Chem. Phys.* **156**, 114117 (2022).
- [30] Aguilar, J. and Combes, J.-M., “A class of analytic perturbations for one-body Schrödinger Hamiltonians”, *Commun. Matz. Phys.* **22**, 269–279 (1971).
- [31] Balslev, E. and Combes, J.-M., “Spectral properties of many-body Schrödinger operators with dilatation-analytic interactions”, *Commun. Matz. Phys.* **22**, 280–294 (1971).
- [32] McCurdy, C. W. and Rescigno, T. N., “Extension of the method of complex basis functions to molecular resonances”, *Phys. Rev. Lett.* **41**, 1364–1368 (1978).
- [33] Moiseyev, N. and Corcoran, C., “Autoionizing states of  $H_2$  and  $H_2^-$  using the complex-scaling method”, *Phys. Rev. A* **20**, 814–817 (1979).
- [34] Cederbaum, L. S., Zobeley, J., and Tarantelli, F., “Giant intermolecular decay and fragmentation of clusters”, *Phys. Rev. Lett.* **79**, 4778–4781 (1997).
- [35] Zobeley, J., Santra, R., and Cederbaum, L. S., “Electronic decay in weakly bound heteroclusters: Energy transfer versus electron transfer”, *J. Chem. Phys.* **115**, 5076–5088 (2001).
- [36] White, A.F., Head-Gordon, M., and McCurdy, C. W., “Complex basis functions revisited: Implementation with applications to carbon tetrafluoride and aromatic N-containing heterocycles within the static-exchange approximation”, *J. Chem. Phys.* **142**, 054103 (2015).
- [37] Brändas, E. and Froehlich, P., “Continuum orbitals, complex scaling problem, and the extended virial theorem”, *Phys. Rev. A* **16**, 2207–2210 (1977).
- [38] Moiseyev, N., Certain, P. R., and Weinhold, F., “Resonance properties of complex-rotated Hamiltonians”, *Mol. Phys.* **36**, 1613–1630 (1978).
- [39] Čížek, J., “On the correlation problem in atomic and molecular systems. calculation of wavefunction components in Ursell-type expansion using quantum-field theoretical methods”, *J. Chem. Phys.* **45**, 4256–4266 (1966).
- [40] Čížek, J., “On the use of the cluster expansion and the technique of diagrams in calculations of correlation effects in atoms and molecules”, *Adv. Chem. Phys.* **14**, 35–89 (1969).
- [41] Shavitt, I. and Bartlett, R. J., *Many-Body Methods in Chemistry and Physics: MBPT and Coupled-Cluster Theory* (Cambridge University Press, 2009).
- [42] Stanton, J. F. and Bartlett, R. J., “The equation of motion coupled-cluster method. A systematic biorthogonal approach to molecular excitation energies, transition probabilities, and excited state properties”, *J. Chem. Phys.* **98**, 7029–7039 (1993).
- [43] Nooijen, M. and Snijders, J. G., “Coupled cluster Green’s function method: Working equations and applications”, *Int. J. Quantum Chem.* **48**, 15–48 (1993).
- [44] Bauch, S. and Bonitz, M., “Theoretical description of field-assisted postcollision interaction in Auger decay of atoms”, *Phys. Rev. A* **85**, 053416 (2012).

- [45] Pisanty, E. and Ivanov, M., “Momentum transfers in correlation-assisted tunneling”, *Phys. Rev. A* **89**, 043416 (2014).
- [46] Driver, T., Champenois, E. G., Cryan, J. P., Li, S., Marinelli, A., Rosenberger, P., Kling, M. F., Ortmann, L., and Landsman, A., “Attosecond Electron Correlation and Molecular Resonance in K-Shell Photoexcitation of Nitric Oxide”, APS Division of Atomic and Molecular Physics Meeting 2020.
- [47] Del Bene, J., Ditchfield, R., and Pople, J. A., “Self-Consistent Molecular Orbital Methods. X. Molecular Orbital Studies of Excited States with Minimal and Extended Basis Sets”, *J. Chem. Phys.* **55**, 2236–2241 (1971).
- [48] Dreuw, A. and Head-Gordon, M., “Single-reference ab initio methods for the calculation of excited states of large molecules”, *Chem. Rev.* **105**, 4009–4037 (2005).
- [49] Epifanovsky, E., Gilbert, A. T. B., Feng, X., Lee, J., Mao, Y., Mardirossian, N., Pokhilko, P., White, A. F., Coons, M. P., Dempwolff, A. L., Gan, Z., Hait, D., Horn, P. R., Jacobson, L. D., Kaliman, I., Kussmann, J., Lange, A. W., Lao, K. U., Levine, D. S., Liu, J., McKenzie, S. C., Morrison, A. F., Nanda, K. D., Plasser, F., Rehn, D. R., Vidal, M. L., You, Z.-Q., Zhu, Y., Alam, B., Albrecht, B. J., Aldossary, A., Alguire, E., Andersen, J. H., Athavale, V., Barton, D., Begam, K., Behn, A., Bellonzi, N., Bernard, Y. A., Berquist, E. J., Burton, H. G. A., Carreras, A., Carter-Fenk, K., Chakraborty, R., Chien, A. D., Closser, K. D., Cofer-Shabica, V., Dasgupta, S., de Wergifosse, M., Deng, J., Diedenhofen, M., Do, H., Ehlert, S., Fang, P.-T., Fatehi, S., Feng, Q., Friedhoff, T., Gayvert, J., Ge, Q., Gidofalvi, G., Goldey, M., Gomes, J., González-Espinoza, C. E., Gulania, S., Gunina, A. O., Hanson-Heine, M. W. D., Harbach, P. H. P., Hauser, A., Herbst, M. F., Vera, M. H., Hodecker, M., Holden, Z. C., Houck, S., Huang, X., Hui, K., Huynh, B. C., Ivanov, M., Jász, A., Ji, H., Jiang, H., Kaduk, B., Kähler, S., Khistyayev, K., Kim, J., Kis, G., Klunzinger, P., Koczor-Benda, Z., Koh, J. H., Kosenkov, D., Koulias, L., Kowalczyk, T., Krauter, C. M., Kue, K., Kunitsa, A., Kus, T., Ladjánszki, I., Landau, A., Lawler, K. V., Lefrancois, D., Lehtola, S., Li, R. R., Li, Y.-P., Liang, J., Liebenthal, M., Lin, H.-H., Lin, Y.-S., Liu, F., Liu, K.-Y., Loipersberger, M., Luenser, A., Manjanath, A., Manohar, P., Mansoor, E., Manzer, S. F., Mao, S.-P., Marenich, A. V., Markovich, T., Mason, S., Maurer, S. A., McLaughlin, P. F., Menger, M. F. S. J., Mewes, J.-M., Mewes, S. A., Morgante, P., Mullinax, J. W., Oosterbaan, K. J., Paran, G., Paul, A. C., Paul, S. K., Pavošević, F., Pei, Z., Prager, S., Proynov, E. I., Rák, A., Ramos-Cordoba, E., Rana, B., Rask, A. E., Rettig, A., Richard, R. M., Rob, F., Rossomme, E., Scheele, T., Scheurer, M., Schneider, M., Sergueev, N., Sharada, S. M., Skomorowski, W., Small, D. W., Stein, C. J., Su, Y.-C., Sundstrom, E. J., Tao, Z., Thirman, J., Tornai, G. J., Tsuchimochi, T., Tubman, N. M., Veccham, S. P., Vydrov, O., Wenzel, J., Witte, J., Yamada, A., Yao, K., Yeganeh, S., Yost, S. R., Zech, A., Zhang, I. Y., Zhang, X., Zhang, Y., Zuev, D., Aspuru-Guzik, A., Bell, A. T., Besley, N. A., Bravaya, K. B., Brooks, B. R., Casanova, D., Chai, J.-D., Coriani, S., Cramer, C. J., Cserey, G., DePrince, A. E., DiStasio, R. A., Dreuw, A., Dunietz, B. D., Furlani, T. R., Goddard, W. A., Hammes-Schiffer, S., Head-Gordon, T., Hehre, W. J., Hsu, C.-P., Jagau, T.-C., Jung, Y., Klamt, A., Kong, J., Lambrecht, D. S., Liang, W., Mayhall, N. J., McCurdy, C. W., Neaton, J. B., Ochsenfeld, C., Parkhill, J. A., Peverati, R., Rassolov, V. A., Shao, Y., Slipchenko, L. V., Stauch, T., Steele, R. P., Subotnik, J. E., Thom, A. J. W., Tkatchenko, A., Truhlar, D. G., Voorhis, T. V., Wesolowski, T. A., Whaley, K. B., Woodcock, H. L., Zimmerman, P. M., Faraji, S., Gill, P. M. W., Head-Gordon, M., Herbert, J. M., and Krylov, A. I., “Software for the frontiers of quantum chemistry: An overview of developments in the Q-Chem 5 package,” *J. Chem. Phys.* **155**, 084801 (2021).
- [50] Bravaya, K. B., Zuev, D., Epifanovsky, E., and Krylov, A. I., “Complex-scaled equation-of-motion coupled-cluster method with single and double substitutions for autoionizing excited states: Theory, implementation, and examples”, *J. Chem. Phys.* **138**, 124106 (2013).
- [51] Zuev, D., Jagau, T.-C., Bravaya, K. B., Epifanovsky, E., Shao, Y., Sundstrom, E., Head-Gordon, M., and Krylov, A. I., “Complex absorbing potentials within EOM-CC family of

- methods: Theory, implementation, and benchmarks”, *J. Chem. Phys.* **141**, 024102 (2014).
- [52] White, A. F., McCurdy, C. W., Head-Gordon, M., “Restricted and unrestricted non-Hermitian Hartree-Fock: Theory, practical considerations, and applications to metastable molecular anions”, *J. Chem. Phys.* **143**, 074103 (2015).
- [53] White, A. F., Epifanovsky, E., McCurdy, C. W., and Head-Gordon, M., “Second-order Møller-Plesset and coupled cluster singles and doubles methods with complex basis functions for resonances in electron-molecule scattering”, *J. Chem. Phys.* **146**, 234107 (2017).
- [54] Gilbert, A. T. B., Besley, N. A., and Gill, P. M. W., “Self-Consistent Field Calculations of Excited States Using the Maximum Overlap Method (MOM)”, *J. Phys. Chem. A* **112**, 13164–13171 (2008).
- [55] Inhester, L., Burmeister, C. F., Groenhof, G., and Grubmüller, H., “Erratum: “Auger spectrum of a water molecule after single and double core ionization” [*J. Chem. Phys.* **136**, 144304 (2012)]”, *J. Chem. Phys.* **141**, 069904 (2014).
- [56] Müller, A., Bernhardt, D., Borovik Jr., A., Buhr, T., Hellhund, J., Holste, K., Kilcoyne, A. L. D., Klumpp, S., Martins, M., Ricz, S., Seltmann, J., Viefhaus, J., and Schippers, S., “Photoionization of Ne atoms and Ne<sup>+</sup> ions near the K edge: Precision spectroscopy and absolute cross-sections”, *Astrophys. J.* **836**, 166 (2017).
- [57] Sankari, R., Ehara, M., Nakatsuji, H., Senba, Y., Hosokawa, K., Yoshida, H., De Fanis, A., Tamenori, Y., Aksela, S., and Ueda, K., “Vibrationally resolved O 1s photoelectron spectrum of water”, *Chem. Phys. Lett.* **380**, 647–653 (2003).
- [58] Carroll, X. T., Berrah, N., Bozek, J., Hahne, J., Kukk, E., Saethre, L. J., and Thomas, T. D., “Carbon 1s photoelectron spectrum of methane: Vibrational excitation and core-hole lifetime”, *Phys. Rev. A* **59**, 3386–3393 (1999).
- [59] Asplund, L., Gelius, U., Hedman, S., Helenelund, K., Siegbahn, K., and Siegbahn, P. E. M., “Vibrational structure and lifetime broadening in core-ionised methane”, *J. Phys. B* **18**, 1569–1579 (1985).
- [60] Heimann, P. A., Medhurst, L. J., Siggel, M. R. F., Shirley, D. A., Chen, C. T., Ma, Y., and Sette, F., “Zero electron kinetic energy photoemission of CH<sub>4</sub> and CD<sub>4</sub> at the carbon K ionization threshold” *Chem. Phys. Lett.* **183**, 234–238 (1991).
- [61] Köppe, H. M., Itchkawitz, B. S., Kilcoyne, A. L. D., Feldhaus, J., Kempgens, B., Kivimäki, A., Neeb, M., and Bradshaw, A. M., “High-resolution C 1s photoelectron spectra of methane”. *Phys. Rev. A* **53**, 4120–4126 (1996).
- [62] McGuire, E. J., “K-Shell Auger Transition Rates and Fluorescence Yields for Elements Be-Ar”, *Phys. Rev.* **185**, 1–6 (1969).
- [63] Hasoğlu, M. F., Nikolić, D., Gorczyca, T. W., Manson, S. T., Chen, M. H., and Badnell, N. R., “Nonmonotonic behavior as a function of nuclear charge of the K-shell Auger and radiative rates and fluorescence yields along the  $1s2s^22p^3$  isoelectronic sequence”, *Phys. Rev. A* **78**, 032509 (2008).
- [64] Jahnke, T., Hergenhahn, U., Winter, B., Dörner, R., Frühling, U., Demekhin, P. V., Gokhberg, K., Cederbaum, L. S., Ehresmann, A., Knie, A., and Dreuw, A., “Interatomic and intermolecular Coulombic decay”, *Chem. Rev.* **120**, 11295–11369 (2020).

# Supplementary Material: Channel-specific core-valence projectors for determining partial Auger decay widths

Florian Matz<sup>1</sup>, Thomas-Christian Jagau<sup>1</sup>

<sup>1</sup>*Division of Quantum Chemistry and Physical Chemistry, KU Leuven, Celestijnenlaan 200F, 3001 Leuven, Belgium*

E-Mail: florian.matz@kuleuven.be; thomas.jagau@kuleuven.be

24th May 2022

Table 1: Exponents used for complex-scaled basis functions in CBF calculations.

Atom	s	p	d
Basis set: cc-pCVTZ (5sp) + 2×(spd)			
H	0.398 893	1.605 600	2.184 213
	0.129 217	0.520 551	0.386 118
C	1.577 501	6.349 666	8.637 909
	0.511 016	2.058 625	1.526 981
N	2.180 490	8.776 783	11.939 692
	0.706 349	2.845 520	2.110 659
O	2.775 914	11.173 450	15.200 051
	0.899 231	3.622 543	2.687 015
Ne	4.330 600	17.431 284	23.713 034
	1.402 856	5.651 395	4.191 912
Basis set: cc-pCVTZ (5sp) + 4×(spd)			
H	0.398 893	1.605 600	2.184 213
	0.258 435	1.041 103	0.772 236
	0.129 217	0.520 551	0.386 118
	0.064 609	0.260 276	0.193 059
O	2.775 914	11.173 450	15.200 051
	1.798 461	7.245 086	5.374 029
	0.899 231	3.622 543	2.687 015
	0.449 615	1.811 272	1.343 507
Ne	4.330 600	17.431 284	23.713 034
	2.805 712	11.302 789	8.383 823
	1.402 856	5.651 395	4.191 912
	0.701 428	2.825 697	2.095 956

Table 2: Results for the core-ionized state of water from CIS calculations using different states of the water cation as HF reference. The cc-pCVTZ (5sp) basis set with 2 complex scaled s-, p- and d-shells on each atom is used.  $\Delta E$  refers to the energy difference between valence-hole reference state and core-ionized state. Calculations were carried out with a  $\theta$  optimized for each reference (upper part of the table) and with a uniform  $\theta$  (lower part of the table). The last row shows the sum of the partial half-widths of the channels included in the respective CIS calculation as obtained from a decomposition of the CCSD energy. Here, only 50% of the width is considered for decay into open-shell singlet states as only 50% of these wave functions is described by CIS.

HF reference state	$2a_1^{-1}$	$1b_2^{-1}$	$3a_1^{-1}$	$1b_1^{-1}$
Decay channels included	$2a_12a_1, 2a_13a_1, 2a_11b_1, 2a_11b_2$	$2a_11b_2, 3a_11b_2, 1b_11b_2, 1b_21b_2$	$2a_13a_1, 3a_13a_1, 3a_11b_1, 3a_11b_2$	$2a_11b_1, 3a_11b_1, 1b_11b_1, 1b_11b_2$
$\theta_{\text{opt}} / ^\circ$	22	28	28	14
$ dE/d\theta  / \text{Hartree}/^\circ$	$4.5 \cdot 10^{-6}$	$1.2 \cdot 10^{-5}$	$1.7 \cdot 10^{-5}$	$2.4 \cdot 10^{-5}$
$\text{Re}(\Delta E) / \text{eV}$	514.0	530.0	533.4	535.1
$-\text{Im}(\Delta E) / \text{meV}$	19.6	11.1	20.1	14.4
$-\text{Im}(E) / \text{meV}$	26.6	16.2	18.4	17.1
$\theta / ^\circ$	28	28	28	28
$ dE/d\theta  / \text{Hartree}/^\circ$	$9.9 \cdot 10^{-6}$	$1.2 \cdot 10^{-5}$	$1.7 \cdot 10^{-5}$	$4.3 \cdot 10^{-5}$
$\text{Re}(\Delta E) / \text{eV}$	514.0	530.0	533.4	535.1
$-\text{Im}(\Delta E) / \text{meV}$	20.0	11.1	20.1	13.6
$-\text{Im}(E) / \text{meV}$	24.8	16.2	18.4	18.1
$\sum \Gamma_{\text{CCSD}}/2 / \text{meV}$	21.7	15.8	19.1	20.6

Table 3: Partial half-widths of core-ionized water, calculated with different methods and the cc-pCVTZ (5sp) basis set with 2 complex scaled s-, p- and d-shells on each atom.

Decay channel	CIS				CCSD ACP “out”	EOMIP-CCSD ACP “out”	CCSD energy decomp. <sup>a</sup>	MRCI Fano <sup>b</sup>	
	ACP/id. $\theta$ “in”	ACP/id. $\theta$ “out”	ACP/diff. $\theta$ “in”	ACP/diff. $\theta$ “out”					
$2a_12a_1$	8.7	8.8	8.8	9.1	9.8	8.5	9.1	9.7	2.1
$2a_13a_1$ (singlet)	7.0	7.2	6.8	7.1	6.6	6.6	6.8	8.6	5.5
$2a_13a_1$ (triplet)	1.2	1.4	1.2	1.4	1.3	1.2	1.3	1.8	1.3
$2a_11b_1$ (singlet)	6.2	6.4	6.3	6.5	6.0	6.1	6.5	7.9	5.0
$2a_11b_1$ (triplet)	1.4	1.5	1.4	1.6	1.5	1.4	1.6	1.9	1.5
$2a_11b_2$ (singlet)	4.4	4.5	4.1	4.2	3.8	4.2	4.1	6.2	3.3
$2a_11b_2$ (triplet)	1.1	1.2	1.0	1.2	1.1	1.0	1.0	1.5	0.8
$3a_13a_1$	5.6	5.7	5.6	5.7	5.1	4.6	5.9	7.3	6.6
$3a_11b_1$ (singlet)	7.8	7.9	7.1	7.2	7.3	6.9	8.3	10.9	9.0
$3a_11b_1$ (triplet)	0.2	0.2	0.2	0.2	0.1	0.1	0.1	0.1	0.2
$3a_11b_2$ (singlet)	6.5	6.6	6.5	6.6	7.2	6.1	8.3	8.3	6.6
$3a_11b_2$ (triplet)	0.1	0.1	0.1	0.1	0.1	0.1	0.1	0.1	0.2
$1b_11b_1$	7.6	7.6	6.7	6.6	7.1	6.4	8.1	9.8	9.5
$1b_11b_2$ (singlet)	6.8	6.9	6.1	6.2	6.0	5.8	6.9	9.1	7.6
$1b_11b_2$ (triplet)	0.0	0.0	0.0	0.0	0.0	0.0	0.0	0.0	0.0
$1b_21b_2$	4.3	4.3	4.3	4.3	4.3	3.9	5.0	5.4	4.9
Sum	68.8	70.5	66.3	67.9	67.3	62.8	73.1	88.5	64.1

<sup>a</sup> Right column: Obtained with the cc-pCVTZ (5sp) basis set with 4 complex scaled s-, p- and d-shells on each atom.

<sup>b</sup> From Refs. 24 and 55.

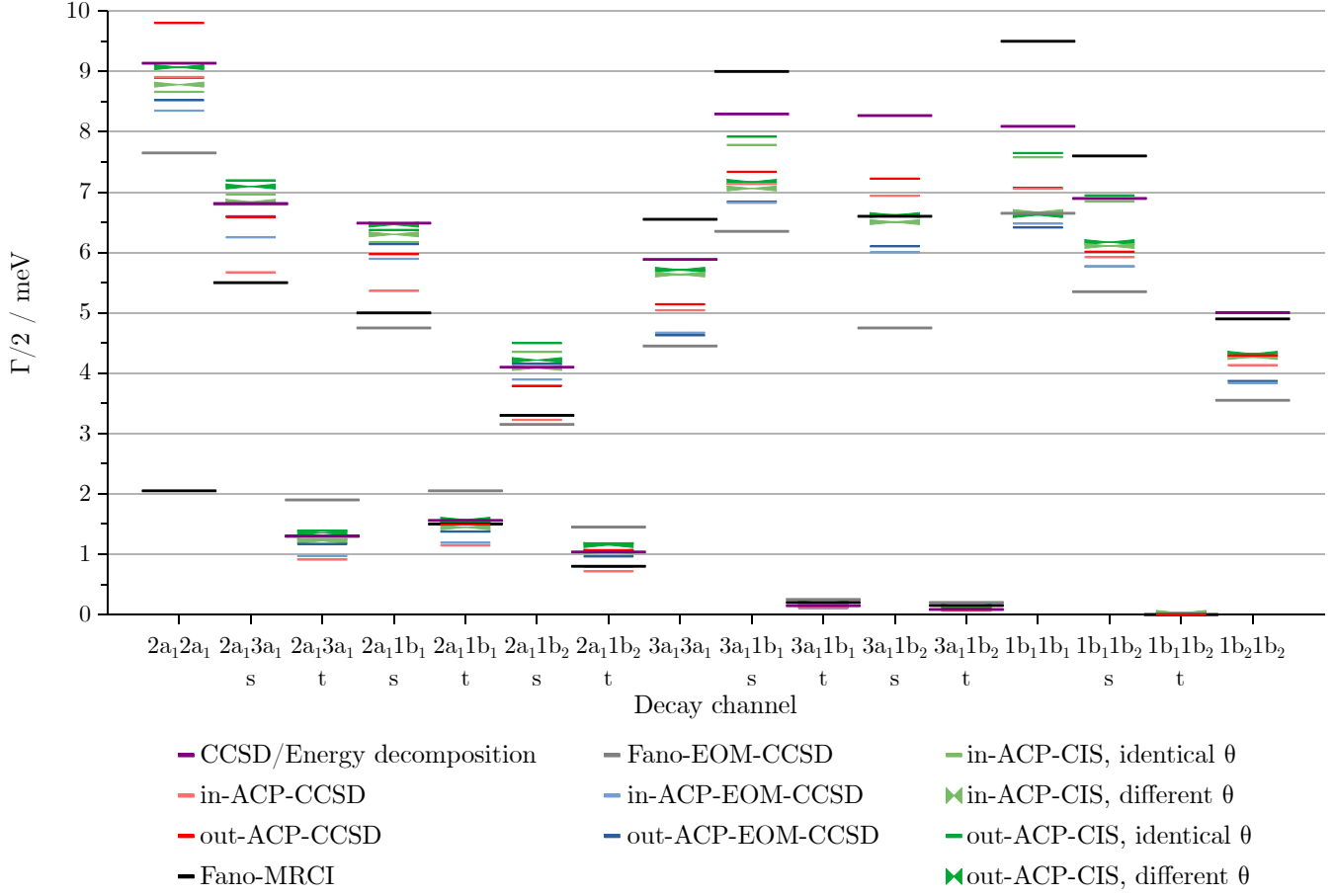


Figure 1: Partial decay widths of core-ionized water computed with different methods. Complex-variable calculations are done with the cc-pCVTZ (5sp) basis set with 2 complex scaled s-, p- and d-shells on each atom; all values are available from Table 3. Fano-MRCI and Fano-EOM-CCSD results are taken from Refs. [24,55] and [26], respectively.

Table 4: Total decay half-widths of the core-ionized neon atom, CIS-“out” (reconstituted) calculated with different methods.

Method	CS/cc-pCV5Z			CBF/cc-pCVTZ (5sp) + 2×(spd)		
	$\theta_{\text{opt}}$ / °	$\frac{dE}{d\theta}$ / Hartree/°	$-\text{Im}(E)$ / meV	$\theta_{\text{opt}}$ / °	$\frac{dE}{d\theta}$ / Hartree/°	$-\text{Im}(E)$ / meV
EOMIP-CCSD	10	$3.3 \cdot 10^{-5}$	102	17	$3.8 \cdot 10^{-5}$	115
$\Delta$ CCSD	12	$3.8 \cdot 10^{-6}$	94	22	$5.4 \cdot 10^{-5}$	129
out-ACP-CIS	9	$2.1 \cdot 10^{-4}$	125	20	$1.1 \cdot 10^{-4}$	107
CIS (2p <sup>-1</sup> )	9	$5.0 \cdot 10^{-5}$	29	20	$2.5 \cdot 10^{-5}$	24
CIS (2s <sup>-1</sup> )	9	$6.2 \cdot 10^{-5}$	28	20	$3.0 \cdot 10^{-5}$	42
Fano-EOM-CCSD <sup>a</sup>	–	–	109	–	–	109
Experiment <sup>b</sup>	–	–	129	–	–	129

<sup>a</sup> From Ref. 26.

<sup>b</sup> From Ref. 56.

Table 5: Total decay half-widths of the core-ionized ammonia and methane molecules, calculated with different methods and the cc-pCVTZ (5sp) basis set with 2 complex scaled s-, p- and d-shells on each atom.

Ammonia			
Method	$\theta_{\text{opt}}/^\circ$	$\frac{dE}{d\theta} / \text{Hartree}/^\circ$	$-\text{Im}(E) / \text{meV}$
EOMIP-CCSD	21	$5.3 \cdot 10^{-6}$	56
$\Delta$ CCSD	15	$8.6 \cdot 10^{-6}$	55
out-ACP-CIS	23	$4.7 \cdot 10^{-5}$	53
Methane			
EOMIP-CCSD	19	$1.5 \cdot 10^{-5}$	37
$\Delta$ CCSD	13	$2.3 \cdot 10^{-5}$	38
out-ACP-CIS	15	$3.2 \cdot 10^{-5}$	37
Fano-EOM-CCSD <sup>a</sup>	–	–	33
Experiment <sup>b</sup>	–	–	47

<sup>a</sup> From Ref. 26.

<sup>b</sup> From Ref. 58.

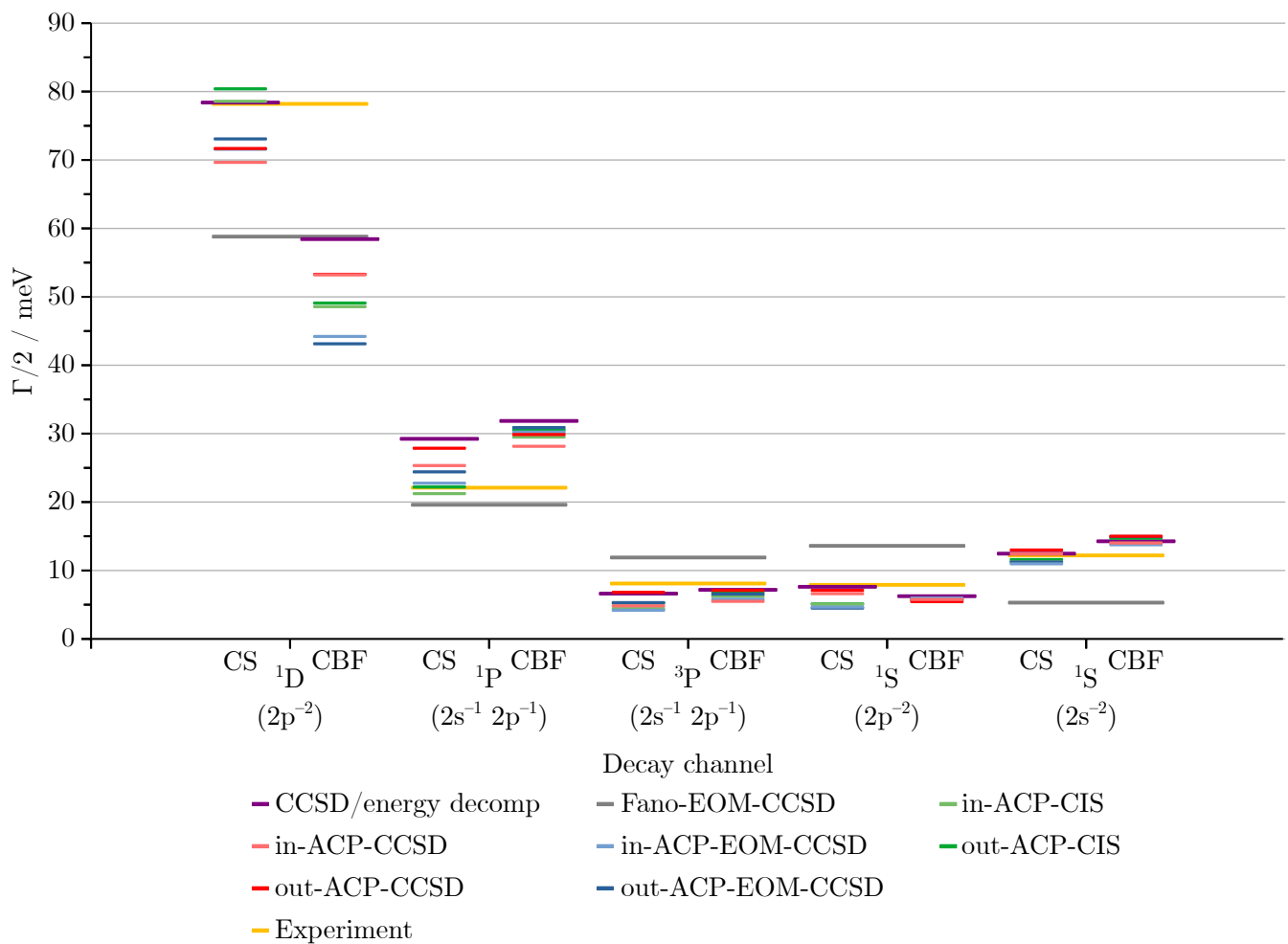


Figure 2: Partial widths of core-ionized neon, calculated with different methods. Experimental values from Ref. 56. Fano-EOM-CCSD values from Ref. 26.

Table 6: Partial half-widths of core-ionized neon, calculated with different methods.

Decay channel	CCSD ACP		EOMIP-CCSD ACP		CIS ACP		CCSD energy decomp.	EOM-CCSD Fano <sup>a</sup>	expt <sup>b</sup>
	“in”	“out”	“in”	“out”	“in”	“out”			
CS/cc-pCV5Z									
<sup>1</sup> D (2p <sup>-2</sup> )	69.6	71.7	71.6	73.1	78.6	80.4	78.4	58.8	78.2(21)
<sup>1</sup> P (2s <sup>-1</sup> 2p <sup>-1</sup> )	25.3	27.9	22.8	24.4	21.2	22.2	29.2	19.6	22.1(7)
<sup>3</sup> P (2s <sup>-1</sup> 2p <sup>-1</sup> )	4.8	6.8	4.2	5.3	4.4	5.2	6.6	11.9	8.1(3)
<sup>1</sup> S (2p <sup>-2</sup> )	6.6	7.1	4.7	4.5	5.1	5.1	7.6	13.6	7.9(3)
<sup>1</sup> S (2s <sup>-2</sup> )	12.4	13.0	11.0	11.2	11.3	11.6	12.5	5.3	12.2(4)
Sum	118.9	126.5	114.2	118.5	120.6	124.5	134.3	109.2	128.5(30)
CBF/cc-pCVTZ (5sp) + 2×(spd)									
<sup>1</sup> D (2p <sup>-2</sup> )	56.3	56.7	44.2	43.1	48.6	49.1	58.4		
<sup>1</sup> P (2s <sup>-1</sup> 2p <sup>-1</sup> )	27.4	29.4	30.2	30.9	29.5	30.5	31.9		
<sup>3</sup> P (2s <sup>-1</sup> 2p <sup>-1</sup> )	5.3	7.2	5.8	6.6	6.2	6.9	7.2		
<sup>1</sup> S (2p <sup>-2</sup> )	5.4	5.1	6.0	5.7	5.8	5.8	6.2		
<sup>1</sup> S (2s <sup>-2</sup> )	13.3	13.8	13.8	15.0	14.0	14.7	14.3		
Sum	107.7	112.2	100.0	101.2	104.1	107.0	118.0		
CBF/cc-pCVTZ (5sp) + 4×(spd)									
<sup>1</sup> D (2p <sup>-2</sup> )	–	69.4	–	63.7	–	68.0	75.5		
<sup>1</sup> P (2s <sup>-1</sup> 2p <sup>-1</sup> )	–	28.1	–	25.8	–	23.0	29.6		
<sup>3</sup> P (2s <sup>-1</sup> 2p <sup>-1</sup> )	–	6.9	–	5.6	–	5.4	6.7		
<sup>1</sup> S (2p <sup>-2</sup> )	–	4.9	–	4.5	–	3.1	5.7		
<sup>1</sup> S (2s <sup>-2</sup> )	–	13.8	–	12.3	–	13.3	13.5		
Sum	–	123.1	–	111.9	–	112.8	131.0		

<sup>a</sup> From Ref. 26.

<sup>b</sup> From Ref. 56.

Table 7: Partial half-widths of core-ionized ammonia, calculated with different methods and the cc-pCVTZ (5sp) basis set with 2 complex scaled s-, p- and d-shells on each atom.

Decay channel	CCSD ACP		EOMIP-CCSD ACP		CIS ACP		CCSD energy decomp.
	“in”	“out”	“in”	“out”	“in”	“out”	
<sup>1</sup> A <sub>2</sub> (2a <sub>1</sub> <sup>-2</sup> )	7.2	7.8	7.0	7.2	7.4	7.6	7.3
<sup>1</sup> E (2a <sub>1</sub> <sup>-1</sup> 1e <sup>-1</sup> )	5.9	7.2	7.3	7.7	7.5	7.7	7.9
<sup>3</sup> E (2a <sub>1</sub> <sup>-1</sup> 1e <sup>-1</sup> )	1.3	2.0	1.5	1.7	2.0	2.1	2.0
<sup>1</sup> A <sub>1</sub> (1e <sup>-2</sup> )	2.6	2.6	2.5	2.5	2.0	1.9	3.6
<sup>1</sup> E (1e <sup>-2</sup> )	9.8	10.2	8.2	8.3	9.4	9.5	11.7
<sup>3</sup> A <sub>2</sub> (1e <sup>-2</sup> )	0.0	0.0	0.1	0.0	0.0	0.0	0.0
<sup>1</sup> A <sub>1</sub> (3a <sub>1</sub> <sup>-2</sup> )	5.6	5.8	4.7	4.8	5.7	5.8	6.7
<sup>1</sup> A <sub>1</sub> (2a <sub>1</sub> <sup>-1</sup> 3a <sub>1</sub> <sup>-1</sup> )	4.2	5.2	4.9	5.3	5.4	5.6	5.3
<sup>3</sup> A <sub>1</sub> (2a <sub>1</sub> <sup>-1</sup> 3a <sub>1</sub> <sup>-1</sup> )	0.7	1.1	0.8	1.0	1.0	1.1	1.1
<sup>1</sup> E (3a <sub>1</sub> <sup>-1</sup> 1e <sup>-1</sup> )	11.6	12.2	10.1	10.3	11.3	11.5	14.2
<sup>3</sup> E (3a <sub>1</sub> <sup>-1</sup> 1e <sup>-1</sup> )	0.1	0.1	0.1	0.1	0.2	0.2	0.1
Sum	49.0	54.2	47.1	48.9	51.9	53.2	59.9



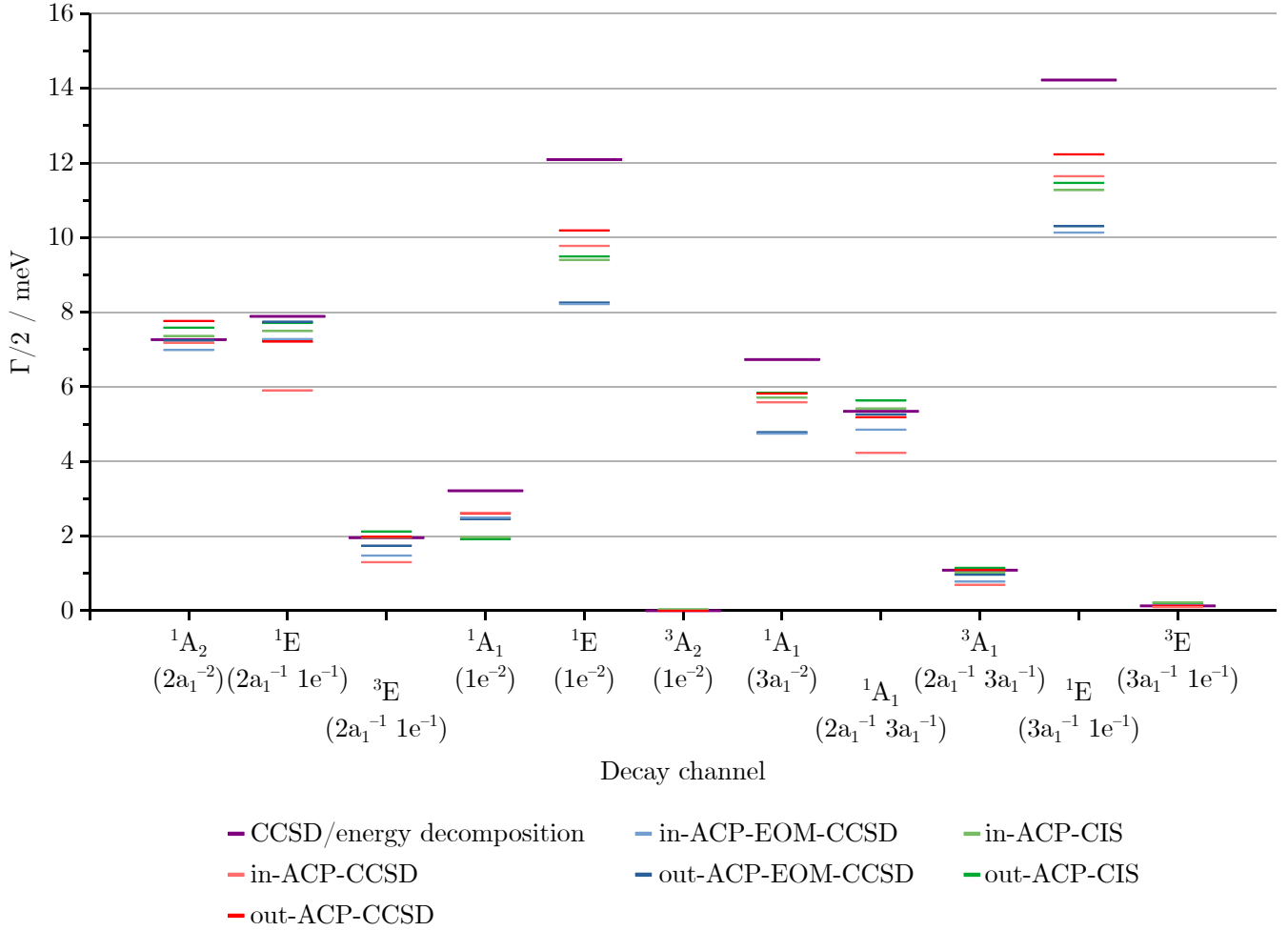


Figure 3: Partial widths of core-ionized ammonia, calculated with different methods and the cc-pCVTZ (5sp) basis set with 2 complex scaled s-, p- and d-shells on each atom.

Table 8: Partial half-widths of core-ionized methane, calculated with different methods and the cc-pCVTZ (5sp) basis set with 2 complex scaled s-, p- and d-shells on each atom.

Decay channel	CCSD ACP		EOMIP-CCSD ACP		CIS ACP		CCSD energy decomp.	EOM-CCSD Fano <sup>a</sup>
	“in”	“out”	“in”	“out”	“in”	“out”		
$^1A_1 (2a_1^{-2})$	5.9	5.9	5.9	5.8	5.8	5.9	5.7	6.6
$^1T_2 (2a_1^{-1}1t_2^{-1})$	6.7	8.6	8.3	8.7	6.7	7.1	9.5	7.1
$^3T_2 (2a_1^{-1}1t_2^{-1})$	1.8	2.9	2.0	2.3	2.1	2.4	2.9	3.4
$^1T_2 (1t_2^{-2})$	14.6	16.3	11.6	12.0	13.6	14.0	19.3	8.0
$^1A_1 (1t_2^{-2})$	1.1	0.9	1.3	1.1	1.3	1.1	1.3	3.0
$^1E (1t_2^{-2})$	7.9	8.3	6.5	6.5	6.3	6.3	9.9	5.4
$^3T_1 (1t_2^{-2})$	0.0	0.0	0.0	0.0	0.1	0.1	0.0	0.0
Sum	38.0	43.0	35.5	36.4	35.9	37.0	48.7	33.4

<sup>b</sup> From. Ref. 26.

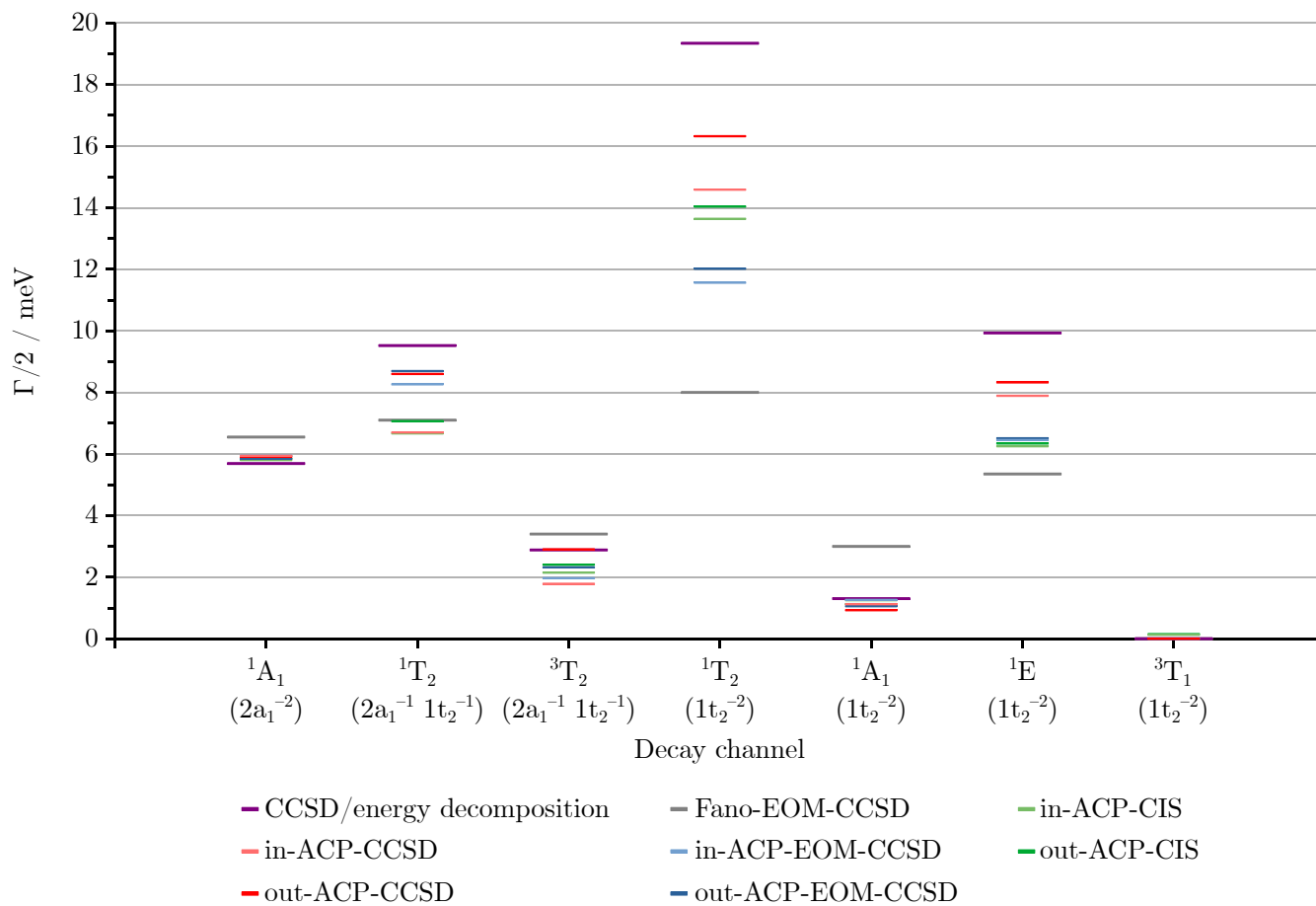


Figure 4: Partial widths of core-ionized methane, calculated with different methods and the cc-pCVTZ (5sp) basis set with 2 complex scaled s-, p- and d-shells on each atom. Fano-EOM-CCSD values from Ref. 26.

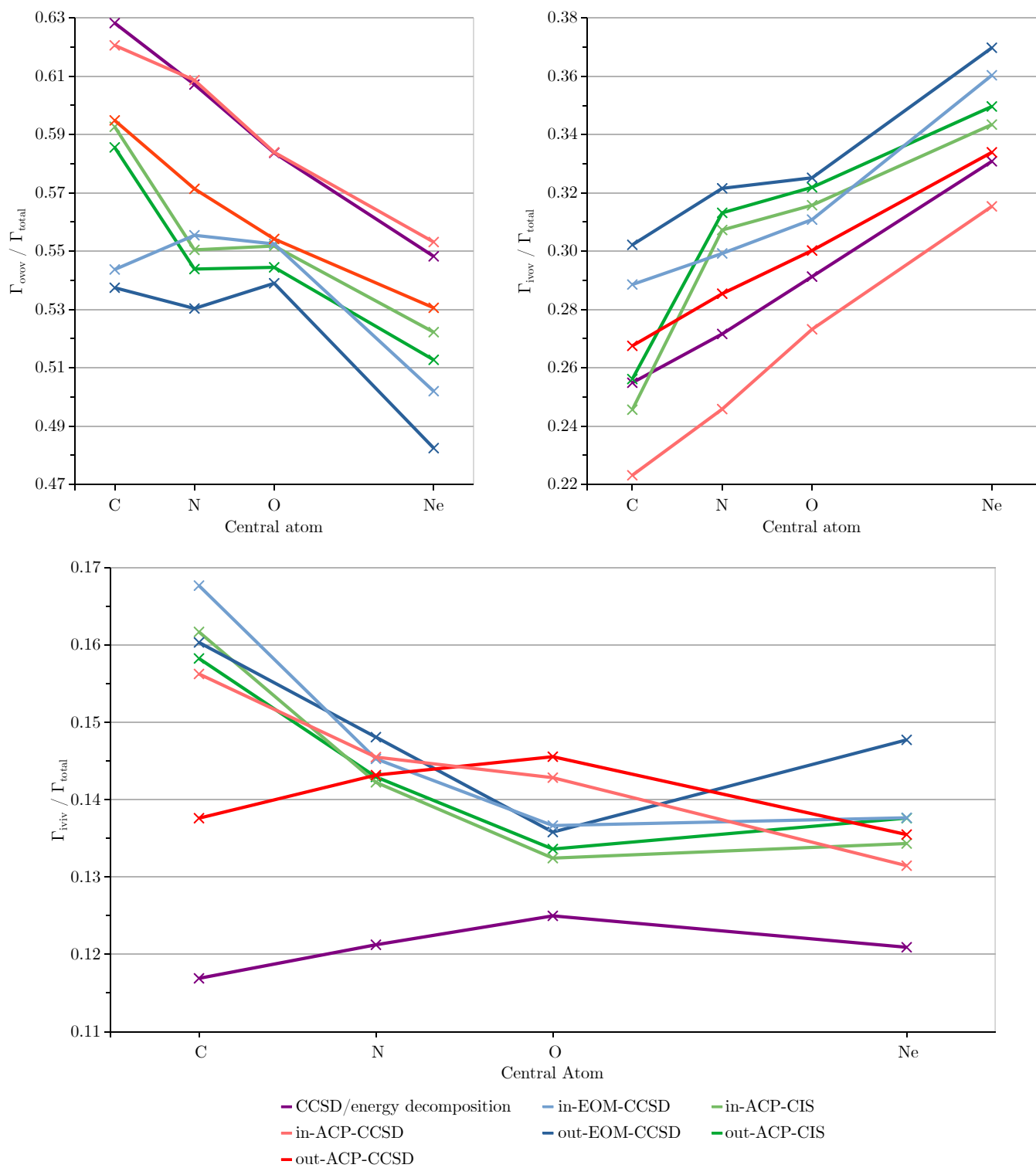


Figure 5: Relative contributions of decay channels involving two outer-valence spin-orbitals (upper left), one outer-valence and one inner-valence spin-orbital (upper right), and two inner-valence spin-orbitals (bottom) to the total Auger decay width of CH<sub>4</sub>, NH<sub>3</sub>, H<sub>2</sub>O, and Ne.